Università degli Studi di Padova

Department of Physics and Astronomy "Galileo Galilei"
Master Degree in Physics

Final Dissertation

Leptonic QED Contributions to Muon-Electron Scattering at NNLO

Thesis Supervisors:
Prof. Massimo Passera

Candidate
Elisa Balzani
Matriculation Number
1205208

Contents

Bibliography   57

Chapter 1

Introduction

The anomalous magnetic moment of the muon, $a_\mu = (g_\mu - 2)/2$, plays an important role in testing the Standard Model (SM) of fundamental interactions. Confirmation of the long-standing muon g-2 discrepancy of $3 - 4\sigma$ requires both experimental and theoretical progress. Moreover, this discrepancy represents one of the most intriguing hints of New Physics(NP) emerged so far in particle physics. On the experimental side, the new E989 Muon g-2 experiment at Fermilab is expected to achieve an unprecedented precision of 0.14 parts-per million (ppm). In addition, a completely new low-energy approach to measuring the g-2 is being developed by the E34 collaboration at J-PARC.

On the theory side, the hadronic correction are under close scrutiny, as they induce the leading uncertainty of the SM prediction of a_μ^{SM}. The calculation of the leading hadronic contribution to the muon g-2, a_μ^{HLO}, traditionally relies on a dispersive integral using the hadronic production cross section in electron-positron annihilation at low energies. Alternative evaluations of a_μ^{HLO} can be obtained via lattice QCD. However, current lattice QCD results are not yet competitive with those obtained with the dispersive approach.

Recently, a new experiment, MUonE, has been proposed at CERN to determine the leading order hadronic contribution to the muon g-2, measuring the effective electromagnetic coupling in the space-like region via scattering data. The elastic scattering of high energy muons on atomic electrons has been identified as an ideal process for this measurement. In order to reach a determination of the hadronic vacuum polarization with a precision below one percent, the shape of the μe differential cross section must be measured with a systematic uncertainty of the order of 10 ppm or better. An analogous precision is therefore required in the theoretical prediction, and the QED corrections at next-to-leading order (NLO) and next-to-next-to-leading order (NNLO) represent a crucial ingredient to interpret the high-precision data of the MUonE experiment. Among the NNLO QED corrections, the "leptonic" ones arise from two-loop diagrams with leptonic vacuum polarization insertions in the photon propagator.

Goal of this thesis is the evaluation of the leptonic NNLO QED contributions to the cross-section of muon-electron scattering. In Chapter 2 we introduce the anomalous magnetic moment of the muon and the current status of the theoretical prediction. In Chapter 3 we discuss the MUonE proposal, studying the differential cross-section for muon-electron elastic scattering. In particular, we analyzed the QED corrections up to NLO, which rep-

resent the benchmark for the evaluation of leptonic NNLO QED corrections. The Chapter 4 is dedicated to the evaluation of the leptonic NNLO QED corrections. In particular, non-factorizable two-loop diagrams were calculated employing the dispersive approach based on the subtracted dispersion relation. Finally, in Chapter 5, we report our conclusions.

Chapter 2

The Muon Anomalous Magnetic Moment

In order to understand what is so special about the muon anomalous magnetic moment we have to look at leptons in general. The muon μ^-, together with the electron e^- and the tau τ^- particle, represent the known charged leptons: elementary spin $1/2$ fermions of electric charge -1 in units of the positron charge e, as a free relativistic one particle state described by the Dirac equation. Of course the charged leptons are never really free, they interact electromagnetically with the photon and weakly via the heavy gauge bosons W and Z. These three leptons differ for the masses which are given by $m_e = 0.511$ MeV, $m_\mu = 105.658$ MeV and $m_\tau = 1776.99$ MeV, respectively.

Beside charge, spin and mass, leptons have other very interesting static (classical) electromagnetic and weak properties like the magnetic and electric dipole moments. Classically the dipole moments can arise from either electrical charges or currents. A well known example is the circulating current, due to an orbiting particle with electric charge e and mass m, which exhibits a magnetic dipole moment given by

$$\vec{\mu}_L = \frac{e}{2m}\vec{L} \tag{2.1}$$

where $\vec{L} = m\vec{r} \times \vec{v}$ is the orbital angular momentum, with $\vec{r}$ and $\vec{v}$ as the position and the velocity of the particle respectively.

Through the replacing of the angular momentum operator $\vec{L}$ with the spin operator

$$\vec{S} = \frac{\vec{\sigma}}{2}, \tag{2.2}$$

we can generalize the classical form (2.1) of the orbital magnetic moment

$$\vec{\mu}_m = g\frac{Qe}{2m}\frac{\vec{\sigma}}{2}, \tag{2.3}$$

where $\sigma_i (i = 1, 2, 3)$ are the Pauli spin matrices, Q is the electrical charge in units of e, $Q = -1$ for the leptons $Q = +1$ for the antileptons. In particular, the Dirac equation in

the presence of an external magnetic field produces an Hamiltonian

$$H = \frac{(\vec{p} - e\vec{A})^2}{2m} + V(r) + \frac{e}{2m}\vec{B}(\vec{L} + g\vec{S}). \tag{2.4}$$

From the equations (2.3) and (2.4) we can define the gyromagnetic ratio g as the relative strength of the intrinsic magnetic dipole moment to the one of the spin-orbit coupling.

The anomalous magnetic moment is an observable which can be relatively easily studied experimentally from the motion of a lepton in an external magnetic field. A first approach to the value of g was given by Goudschmidt and Uhlenbeck [1] in 1925. They postulated that an electron had an intrinsic angular momentum of $1/2$, associated with a magnetic dipole moment equal to $\frac{e}{2m}$.[1] This set the first prediction of $g = 2$, twice the value of $g = 1$ predicted by classical mechanics. On the experimental side, Back and Landé [2] carried out numerous experimental investigations on the Zeeman effect to verify the Goudschmidt and Uhlenbeck's value, nevertheless they were not really able to determine g.

In 1928 Dirac presented his relativistic theory, which predicted $g = 2$ for a free electron [3]. After first experimental confirmations of Dirac's prediction $g_e = 2$ for the electron (thanks to Kinster and Houston in 1934 [4]), which strongly supported the Dirac theory, yet within relatively large experimental errors at the time, it took about twenty more years of experimental efforts to establish the the electrons magnetic moment actually exceeds 2 by about 0.12%, the first clear indication of the existence of an "anomalous" contribution

$$a_\ell \equiv \frac{g_\ell - 2}{2}, \quad (\ell = e, \mu, \tau) \tag{2.5}$$

to the magnetic moment. By the end of 1940's the breakthrough in understanding and handling renormalization of QED had made explicit predictions of higher order effects possible, and in particular of the leading contribution to the anomalous magnetic moment

$$a_\ell^{QED} = \frac{\alpha}{2\pi}, \quad (\ell = e, \mu, \tau) \tag{2.6}$$

by Schwinger in 1948 [5]. This contribution is due to quantum fluctuations via virtual electron photon interactions and in QED is universal for all leptons.

2.1 The Standard Model Prediction of the Muon g-2

The evaluation of the Standard Model (SM) prediction for the anomalous magnetic moment of the muon a_μ has occupied many physicists for over seventy years. Even if the agreement of the QED leading contribution for a_e with the experimental results provide one of the early confirmations of this theory, the anomalous magnetic moment of the electron is rather insensitive to strong and weak interactions and to yet unknown Beyond SM (BSM) physics, especially at higher energy scales. On the other hand, a_μ allows to test the entire SM and, compared with a_e, it is much better suited to unveil or constrain

---

[1]In this thesis we will use the natural units $\hbar = c = 1$
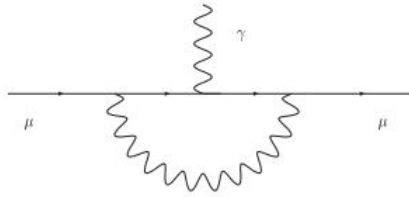
Figure 2.1: Lowest-order QED contribution to a_μ

"new physics" effects. For a lepton ℓ, the contribution to a_ℓ is generally proportional to m_ℓ^2/Λ^2, where m_ℓ is the mass of the lepton and Λ the scale of "new physics", thus leading to an $(m_\mu/m_e)^2 \sim 4 \times 10^4$ relative enhancement of the sensitivity of the muon versus the electron anomalous magnetic moment.

In this chapter we will provide a review of the theoretical prediction for a_μ in the SM, analyzing the three contributions into which a_μ^{SM} is usually split: QED, electroweak (EW) and hadronic.

2.1.1 The QED contribution to a_μ

The QED contribution to the anomalous magnetic moment of the muon arises from the subset of SM diagrams containing only the interaction between leptons (e, μ, τ) and photons. As a dimensionless quantity, it can be cast in the following general form

$$a_\mu^{QED} = A_1 + A_2(m_\mu/m_e) + A_2(m_\mu/m_\tau) + A_3(m_\mu/m_e, m_\mu/m_\tau) \qquad (2.7)$$

where m_e, m_μ and m_τ are the masses of the electron, muon and tau, respectively. The term A_1, arising from diagrams containing only photons and muons, is mass independent. In contrast, the terms A_2 and A_3 are functions of the indicated mass ratios, and are generated by graphs containing also electrons and taus. The renormalizability of QED guarantees that the functions $A_i(i = 1, 2, 3)$ can be expanded as power series in α/π and computed order-by-order

$$A_i = A_i^{(2)}\left(\frac{\alpha}{\pi}\right) + A_i^{(4)}\left(\frac{\alpha}{\pi}\right)^2 + A_i^{(6)}\left(\frac{\alpha}{\pi}\right)^3 + A_i^{(8)}\left(\frac{\alpha}{\pi}\right)^4 + A_i^{(10)}\left(\frac{\alpha}{\pi}\right)^5 + ... \qquad (2.8)$$

By 2018, all terms up to the eighth order have been obtained and cross-checked by different groups using different methods. On the other hand, the entire tenth-order contribution has been calculated only by one group with numerical means. Some of small portions of the tenth-order contribution have been independently double-checked. In the following sections, we summarize all perturbative coefficients $A_i^{(2n)}$ up to the tenth order.

A. One-Loop contribution

Only one diagram, shown in figure 2.1, is involved in the evaluation of the lowest-order contribution; it provides the famous result by Schwinger [5], $A_1^{(2)} = 1/2$ $(A_2^{(2)} = A_3^{(2)} = 0)$.

Let's recall some features about the Lorentz structure of the QED vertex by means of a Lorentz decomposition

$$\Gamma^\mu = \bar{u}(p')\Big[a_1\gamma^\mu + a_2 p^\mu + a_3 p'^\mu\Big]u(p) \tag{2.9}$$

where we assign a four-momentum p to the incoming muon and a four-momentum p' to the outgoing one, so we can define the transfer momentum $q \equiv p' - p$. The coefficients a_i are called form factors. Exploiting the Ward identity we can write

$$0 = q_\mu\Gamma^\mu = \bar{u}(p')\Big[a_1\slashed{q} + a_2 p\cdot q + a_3 p'\cdot q\Big]u(p) \tag{2.10}$$

The term proportional to a_1 vanishes because $\bar{u}(p')(\slashed{p}' - \slashed{p})u(p) \propto m - m = 0$; moreover

$$\begin{aligned}
q\cdot p &= (p' - p)\cdot p = p'\cdot p - m^2, \\
q\cdot p' &= (p' - p)\cdot p' = m^2 - p'\cdot p = -q\cdot p,
\end{aligned} \tag{2.11}$$

therefore we discover that $a_2 = a_3$. Thus there are only two independent form factors and the vertex takes the form

$$\Gamma^\mu = \bar{u}(p')\Big[a_1\gamma^\mu + a_2(p^\mu + p'^\mu)\Big]u(p) \tag{2.12}$$

Now we exploit the Gordon Identity[2] in order to get a decomposition into current and spin density part for the evaluated bilinear.
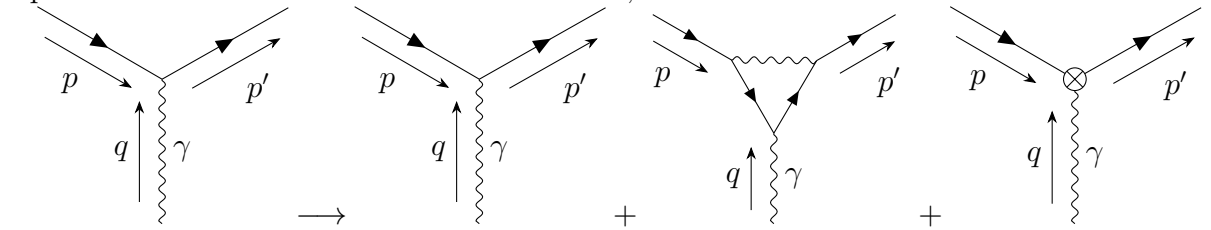
$$\bar{u}(p')(p + p')u(p) = \bar{u}(p')(2m\gamma^\mu - i\sigma^{\mu\nu}q_\nu)u(p) \tag{2.13}$$

Consequently we can rewrite our vertex redefining the form factors as

$$\Gamma^\mu = \bar{u}(p')\Big[F_1(q^2)\gamma^\mu + \frac{F_2(q^2)}{2m}i\sigma^{\mu\nu}q_\nu\Big]u(p). \tag{2.14}$$

The chosen normalization of the second form factor comes from the fact that we want to recover, at the tree level, that $F_1(q^2) = 1$ and $F_2(q^2) = 0$. In particular, in the static limit, defined by $q \to 0$, one obtains $F_1(0) = 1$ and $F_2(0) = a_\mu$, where the first expression is usually called the charge renormalization condition, while the second is the finite prediction for a_μ.

Now we can start the renormalization procedure for the QED vertex, adding the one-loop contribution and the relative counterterm, as follow:


$$\bar{u}(p')ie_0\gamma^\mu u(p) \longrightarrow \bar{u}(p')ie\Big[\gamma^\mu + e^2 f_1(q^2)\gamma^\mu + \frac{e^2}{2m}f_2(q^2)i\sigma^{\mu\nu}q_\nu + (Z_V - 1)\gamma^\mu\Big]u(p) \tag{2.15}$$

---

[2]Since we know that $\{\gamma^\mu, \gamma^\nu\} = 2\eta^{\mu\nu}$ and $\sigma^{\mu\nu} = \frac{i}{2}[\gamma^\mu, \gamma^\nu]$

Notice that the counterterm is proportional to γ^μ only: this implies that the UV divergent behaviour of the one-loop vertex correction is contained in the $f_1(q^2)$ part, while $f_2(q^2)$ is finite.

At this point we are ready to compute the loop integral, in order to renormalize the UV divergence we work in d dimensions
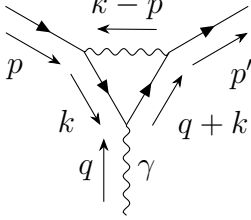
$$ie^2\bar{u}(p')\Gamma^\mu u(p) = (ie^2\mu^{\frac{\epsilon}{2}})^3 \int \frac{d^d k}{(2\pi)^d} \frac{\bar{u}(p')\gamma^\nu(\slashed{q}+\slashed{k}+m)\gamma^\mu(\slashed{k}+m)\gamma_\nu u(p)}{[(k-p)^2-\lambda^2][(q+k)^2-m^2][k^2-m^2]} \qquad (2.16)$$

where μ represents the 't Hoft mass parameter with $\epsilon = 4 - d$, k is the loop momentum and λ is the fictitious mass of the photon, introduced to regularize the IR divergences. In the equation (2.16) we have defined the denominator in such a way that we can exploit the following parametrization

$$\frac{1}{ABC} = 2 \int_0^1 dxdydz\delta(x+y+z-1)\frac{1}{[Ax+By+Cz]^3} \qquad (2.17)$$

with

$$Ax + By + Cz = k^2 + 2k(yq - zp) + yq^2 + zp^2 - (x+y)m^2 = (k + yq - zp)^2 - \Delta \quad (2.18)$$

where we have completed the squared with the remaining terms $\Delta = -xyq^2 + (1-z)^2 m^2$. We are ready to perform the shift $k^\mu \to k^\mu - yq^\mu + zp^\mu$ so that the denominator becomes just $(k^2 - \Delta)$.

Regarding the numerator, we can contract the two gamma matrices and perform again the shift, neglecting linear terms in k obtaining

$$N^\mu = [k^2 - 2(1-x)(1-y)q^2 - 2(1-4z+z^2)m^2]\bar{u}(p')\gamma^\mu u(p)$$
$$-2imz(1-z)q_\nu\bar{u}(p')\sigma^{\mu\nu}u(p) - 2m(z-2)(x-y)q^\mu\bar{u}(p')u(p). \qquad (2.19)$$

The last term on the second line is independent on k and, when integrated over the parametrization, gives a null contribution. Therefore we can split our one-loop integral in two contributions, namely the two form factors

$$e^2 f_1(q^2) = -2ie^2 \int_0^1 dxdydz\delta(x+y+z-1) \int \frac{d^4 k}{(2\pi)^4} \frac{k^2 - 2(1-x)(1-y)q^2 - 2(1-4z+z^2)m^2}{(k^2-\Delta)^3}$$

$$e^2 f_2(q^2) = \frac{2m}{e}(4ie^3 m) \int_0^1 dxdydz\delta(x+y+z-1) \int \frac{d^4 k}{(2\pi)^4} \frac{z(1-z)}{(k^2-\Delta)^3}$$

$$(2.20)$$

The only UV divergent term is the one proportional to k^2 in the $f_1(q^2)$ form factor, indeed it carries a log divergence. All the other terms are k independent, hence are proportional to the integral,

$$\int \frac{d^4k}{(2\pi)^4} \frac{1}{(k^2 - \Delta)^3} = -\frac{i}{32\pi^2\Delta} \tag{2.21}$$

and are UV finite, as one can deduce by dimensional arguments.

Since the gyromagnetic factor is defined in the static limit $q^2 \to 0$, we can compute the integral in this limit

$$e^2 f_2(0) = \frac{\alpha}{\pi} \int_0^1 dx \int_0^1 dy \int_0^1 dz \delta(x+y+z-1) \frac{z}{1-z} = \begin{cases} 0 & if \ 1-y-z = x \notin [0,1] \\ \frac{\alpha}{\pi}n & if \ -z < y < 1-z \end{cases} \tag{2.22}$$

with

$$n = \int_0^1 dz \frac{z}{1-z} \int_0^{1-z} dy = \int_0^1 z = \frac{1}{2} \tag{2.23}$$

Therefore:

$$F_2(0) = e^2 f_2(0) = \frac{\alpha}{2\pi}. \tag{2.24}$$

As we mentioned before this represents the one-loop QED contribution to a_μ.

B. Higher-order QED contributions

The fourth order QED corrections to a_μ are made up by nine diagrams. Among them seven contribute to $A_1^{(4)}$, they are obtained attaching two virtual photons to the muon lines and one is related to the insertion of a vacuum polarization. The remaining two diagrams contribute to $A_2^{(4)}(m_\mu/m_e)$ and $A_2^{(4)}(m_\mu/m_\tau)$, thanks to the insertion of a vacuum polarization loop in the virtual photon line.

The analytic results for the coefficient had been known for almost sixty years [6, 7]. Actually, they can be greatly simplified by taking advantage of the properties of the dilogarithm[3]. One gets [8, 9]

$$A_1^{(4)} = -0.328\ 478\ 965\ 579...$$
$$A_2^{(4)}(m_\mu/m_e) = 1.094\ 258\ 3093\ (76)... \tag{2.25}$$
$$A_2^{(4)}(m_\mu/m_\tau) = 0.000\ 078\ 076\ (11)...,$$

where the standard uncertainties are only caused by the experimental uncertainties of the lepton mass ratio. As there are no two-loop diagrams containing both virtual electrons and taus, $A_3^{(4)}(m_\mu/m_e, m_\mu/m_\tau) = 0$. Summing up all the results in the equation (2.25), one gets the two-loop QED coefficient [8, 9]

$$C_2 = A_1^{(4)} + A_2^{(4)}(m_\mu/m_e) + A_2^{(4)}(m_\mu/m_\tau) = 0.765\ 857\ 419\ (77). \tag{2.26}$$

The uncertainties in $A_2^{(4)}(m_\mu/m_e)$ and $A_2^{(4)}(m_\mu/m_\tau)$ have been added in quadrature. The resulting error $\delta C_2 = 7.7 \times 10^{-8}$ leads to a tiny 0.04×10^{-11} uncertainty in a_μ^{QED}.

---

[3] $Li_2(z) = -\int_0^z dt \frac{\log(1-t)}{t}$

The evaluation of the three-loop (sixth-order) QED contribution involves more than one hundred diagrams. The coefficient $A_1^{(6)}$ arises from 72 diagrams, its calculation in closed analytic form is mainly due to Remiddi and his collaborators[10, 11]. The result reads [8, 9]

$$A_1^{(6)} = 1.181\ 241\ 4566... \tag{2.27}$$

The calculation of the exact expression for the coefficient $A_2^{(6)}(m/M)$, that for our analysis $m = m_\mu$ and $M = m_e$ or m_τ, can be further split into two parts: the first one receives contributions from 36 diagrams containing electron or τ vacuum polarization loops [12], meanwhile the second one is due to 12 light-by-light scattering diagrams with electron or τ loops [13]. The exact expression for $A_2^{(6)}(m/M)$ in closed analytic form is a bit complicated due to the fact that it contains hundreds of polylogarithmic functions up to fifth degree and complex arguments. As a result [8, 9]:

$$
\begin{aligned}
A_2^{(6)}(m_\mu/m_e) &= 22.868\ 379\ 98\ (20), \\
A_2^{(6)}(m_\mu/m_\tau) &= 0.000\ 360\ 671\ (94).
\end{aligned}
\tag{2.28}
$$

The analytic result, for the three-loop diagrams with both electron and τ loop insertion in the photon propagator, yields the numerical value [8, 9]

$$A_3^{(6)}(m_\mu/m_e, m_\mu/m_\tau) = 0.000\ 527\ 738\ (75) \tag{2.29}$$

providing a small 0.7×10^{-11} contribution to a_μ^{QED}. The error, 7.5×10^{-7}, is caused by the uncertainty of the ratio m_μ/m_τ. Combining the three-loop results presented above, one obtains the sixth-order QED coefficient [8, 9]

$$C_3 = A_1^{(6)} + A_2^{(6)}(m_\mu/m_e) + A_2^{(6)}(m_\mu/m_\tau) + A_3^{(6)}(m_\mu/m_e, m_\mu/m_\tau) = 24.050\ 509\ 94\ (122). \tag{2.30}$$

The error $\delta C_3 = 1.2 \times 10^{-6}$, due to the measurement uncertainties of the lepton masses, induces a negligible $O(10^{-14})$ uncertainty in a_μ^{QED}. In parallel to these analytic results, numerical methods were also developed for the evaluation of the full set of three-loop diagrams.

More than one thousand diagrams enter the evaluation of the four-loop QED contribution to a_μ. As only few of them are known analytically [14], this eighth-order term has thus far been evaluated only numerically by Kinoshita and his collaborators [15, 16]. Recently, the eighth-order mass-independent contribution $A_1^{(8)}$ has been calculated in analytical form by Laporta [17]. Since this eighth-order QED contribution is about six times larger than the present experimental uncertainty of a_μ, it is crucial for the comparison between the SM prediction of a_μ and its experimental determination. There are 891 four-loop diagrams contributing to the mass-independent coefficient, the updated result, obtained up to 1100 digits, is [9, 17]

$$A_1^{(8)} = -1.912\ 245\ 764\ 926... \tag{2.31}$$

The latest value of the coefficient $A_2^{(8)}(m_\mu/m_e)$, arising from 469 diagrams, is [18]

$$A_2^{(8)}(m_\mu/m_e) = 132.6823\ (72). \tag{2.32}$$

The eighth-order τ-lepton contributions, $A_2^{(8)}(m_\mu/m_\tau)$ and $A_3^{(8)}(m_\mu/m_e, m_\mu/m_\tau)$, are also independently checked. This is done in two ways, first by numerical calculation [19] and second by use of asymptotic expansion [20],

$$
\begin{aligned}
A_2^{(8)}(m_\mu/m_\tau) &= 0.042\ 4941\ (53), \\
A_3^{(8)}(m_\mu/m_e, m_\mu/m_\tau) &= 0.062\ 722\ (10),
\end{aligned}
\tag{2.33}
$$

which provide a small $O(10^{-12})$ contribution to a_μ^{QED}.

Summing up the four-loop results described above, we obtain the eighth-order QED coefficient [8, 9]

$$
C_4 \simeq A_1^{(8)} + A_2^{(8)}(m_\mu/m_e) + A_2^{(8)}(m_\mu/m_\tau) + A_3^{(8)}(m_\mu/m_e, m_\mu/m_\tau) = 130.876\ 170\ (81).
\tag{2.34}
$$

At tenth order in QED there are more than ten thousand diagrams five-loop contributing to a_μ. The numerical results for the sum of all diagrams with one or more fermion loops are given by [9]:

$$
\begin{aligned}
A_1^{(10)} &= 6.737\ (159), \\
A_2^{(10)}(m_\mu/m_e) &= 742.32\ (86), \\
A_2^{(10)}(m_\mu/m_\tau) &= -0.0656\ (45), \\
A_3^{(10)}(m_\mu/m_e, m_\mu/m_\tau) &= 2.011\ (10), \\
C_5 &= 751.0024\ (169),
\end{aligned}
\tag{2.35}
$$

where all the uncertainties are attributed entirely to the statistical fluctuation in the Monte-Carlo integration of Feynman amplitudes.

C. The numerical value of a_μ^{QED}

Adding up all the above contributions and using the latest recommended value for the fine-structure constant, that comes from Cs atom-interferometry experiment [21],

$$
\alpha^{-1} = 137.035\ 999\ 046\ (27),
\tag{2.36}
$$

The updated value for the QED contribution to the muon g-2 is [9]

$$
a_\mu^{QED} = 116\ 584\ 718.931\ (7)\ (17)\ (6)\ (100)\ (23)\ [104] \times 10^{-11}.
\tag{2.37}
$$

Where the uncertainties are due to τ-lepton mass m_τ, the eighth-order QED, the tenth-order QED, the estimate of the twelfth-order QED, the fine structure constant α, and the sum in quadrature of all of these.

2.1.2 The electroweak contribution

Contrary to the QED effects, the electroweak (EW) contribution to the anomalous magnetic moment of the muon is suppressed by a factor (m_μ^2/M_W^2). The one-loop part was computed in 1972 by several authors [22].

A.   One-loop contribution

The one-loop EW contribution to a_μ is characterized by the analytic expression

$$a_\mu^{EW}(one-loop) = \frac{5G_F m_\mu^2}{24\sqrt{2}\pi^2}\left[1 + \frac{1}{5}(1 - 4\sin^2\theta_w)^2 + O\left(\frac{m_\mu^2}{M_{Z,W,H}^2}\right)\right], \qquad (2.38)$$

where $G_F = 1.16637(1) \times 10^{-5}$ GeV^{-2} is the Fermi coupling constant, M_Z, M_W and M_H are the masses of the Z, W and Higgs boson, and θ_w is the weak mixing angle. Taking into account the fact that the contribution of the Higgs boson to $a_\mu^{EW}(one-loop)$ is of order $O(10^{-14})$, it can be safely neglected, obtaining [9]

$$a_\mu^{EW}(one-loop) = 194.79\ (1) \times 10^{-11}. \qquad (2.39)$$

B.   Higher-order contributions

The two-loop EW contribution to a_μ was computed in 1995 by Czarnecki *et al* [23, 24]. Naively one would expect the two-loop EW contribution to be of order $(\alpha/\pi) \times a_\mu^{EW}(two-loop)$, and thus negligible, but this turns out not to be so. In fact, $a_\mu^{EW}(two-loop)$ is quite substantial because of the appearance of terms enhanced by a factor of $\log(M_{Z,W}/m_f)$, where m_f is a fermion mass scale much smaller than M_W.

We can divide the two-loop contributions into fermionic and bosonic parts; the former includes all two-loop EW corrections containing closed fermion loops, whereas all others are grouped into the latter. The full two-loop calculation involves 1678 diagrams in the linear 't Hooft-Feynman gauge [25]. In particular, we can subdivide the fermionic two-loop contributions into:

$$a_\mu^{EW}(two-loop, ferm.) = a_\mu^{EW(2)}(e, \mu, u, c, d, s) + a_\mu^{EW(2)}(\tau, t, b) + a_{\mu,H}^{EW(2)} + a_{\mu,rest}^{EW(2)} \quad (2.40)$$

The first two terms of the RHS of (2.40) yields respectively [26]

$$\begin{aligned}
a_\mu^{EW(2)}(e, \mu, u, c, d, s) &= -6.91\ (20)\ (30) \times 10^{-11}, \\
a_\mu^{EW(2)}(\tau, t, b) &= -9.21\ (10) \times 10^{-11}.
\end{aligned} \qquad (2.41)$$

The uncertainties are obtained by varying respective input parameters of the hadronic model and perturbative calculations. The hadronic uncertainties, above estimated to be $\sim 2 \times 10^{-11}$, arise from two types of two-loop diagrams: hadronic photon-Z mixing, and quark triangle loops with the external photon, a virtual photon and a Z attached to them. The tiny hadronic $\gamma - Z$ mixing terms can be evaluated either in the free quarks approximation or via a dispersion relation using data from e^+e^- annihilation into hadrons.

The third term of (2.40) denotes the Higgs-dependent fermion loop diagrams, an exact expression can be found in [27]

$$a_{\mu,H}^{EW(2)} = -1.51\ (1) \times 10^{-11}, \qquad (2.42)$$

where the indicated uncertainty arises essentially from the uncertainty of the input parameters m_τ and M_H. The fourth term of (2.40) collects all remaining fermionic two-loop contributions, e.g. W boson exchange [27]

$$a_{\mu,rest}^{EW(2)} = -4.64\ (10) \times 10^{-11}. \qquad (2.43)$$

The bosonic two-loop contributions $a_\mu^{EW}(two-loop, boson)$ are defined by two-loop and associated counterterm diagrams without closed fermion loops, yielding [9, 28]

$$a_{\mu,bos.}^{EW(2)} = -19.96 \ (1) \times 10^{-11}. \tag{2.44}$$

The given theory error is the parametric uncertainty resulting from the experimental uncertainty of the Higgs boson and W-boson masses, using the PDG value $M_H = 125.18(16)$GeV [29].

Summing up the quoted results, one obtains [9]

$$a_\mu^{EW} = 153.6 \ (1) \times 10^{-11}. \tag{2.45}$$

2.1.3   The hadronic contribution

In this section we will analyze the contribution to the muon g-2, which originates from QED diagrams involving hadrons. Hadronic effects in two-loop EW contributions are already included in a_μ^{EW} in the previous section.

In particular, the most consistent hadronic effect is the $O(\alpha^2)$ hadronic vacuum polarization (HVP) insertion on in the internal photon line of the leading one-loop muon vertex diagram.

A.   Leading-order hadronic contribution

The leading hadronic contribution to the muon g-2 is due to the hadronic vacuum polarization insertion in the internal photon propagator of the one-loop diagram. The evaluation of this $O(\alpha^2)$ diagram involves long-distance QCD for which perturbation theory cannot be employed. However, Bouchiat and Michael [30], using analyticity and unitarity, showed that this contribution can be computed from hadronic e^+e^- annihilation data via the dispersion integral [4]

$$a_\mu^{HLO} = \frac{1}{4\pi^3} \int_{4m_\pi^2}^\infty ds K(s)\sigma^{(0)}(s) = \frac{\alpha^2}{3\pi^2} \int_{4m_\pi^2}^\infty \frac{ds}{s} K(s)R(s), \tag{2.46}$$

where $\sigma^{(0)}(s)$ is the experimental total cross section for e^+e^- annihilation into any hadronic state, with extraneous QED radiative corrections subtracted off, and $R(s)$ is the ratio of $\sigma^{(0)}(s)$ and the high-energy limit of the Born cross section for μ-pair production: $R(s) = \sigma^{(0)}(s)/(4\pi\alpha^2/3s)$. The kernel $K(s)$ is a well-known function

$$K(s) = \int_0^1 dx \frac{x^2(1-x)}{x^2 + (s/m_\mu^2)(1-x)}. \tag{2.47}$$

It decreases monotonically for increasing s, and for large s it behaves as $m_\mu^2/3s$ to a good approximation. For this reason the low-energy region of the dispersive integral is enhanced by $\sim 1/s^2$.

---

[4]Details of dispersion integrals will be treated in Chapter 4

Therefore (2.46) offers an approach to overcome long-distance QCD issues appearing in the LO hadronic contribution to the a_μ calculation. Since it makes use of hadronic e^+e^- annihilation data, thus involving a positive squared momentum transfer, we will call it time-like approach.

Detailed evaluations of the dispersive integral (2.46) have been carried out by several authors. The hadronic contribution a_μ^{HLO} is of order 7000×10^{-11} and, even if this is a small fraction of the total SM prediction for a_μ, it is very large compared with the current experimental uncertainty $\delta a_\mu^{exp} = 60 \times 10^{-11}$. Here we only focus on the most recent evaluation from [9, 31, 32]

$$a_\mu^{HLO} = 6931\ (40) \times 10^{-11} \tag{2.48}$$

where the error is due to the experimental measurement of hadronic e^+e^- annihilation.

B.   Higher-order hadronic contributions

We will now briefly discuss the $O(\alpha^3)$ hadronic contribution to the muon g-2, a_μ^{HHO}, which can be divided into two parts:

$$a_\mu^{HHO} = a_\mu^{HHO}(vp) + a_\mu^{HHO}(lbl). \tag{2.49}$$

The first is the $O(\alpha^3)$ contribution of diagrams containing hadronic vacuum polarization insertions, while the second one is the light-by-light contribution. In recent years, $a_\mu^{HHO}(vp)$ was evaluated by Keshavarzi *et al.* [32]

$$a_\mu^{HHO} = -98.3\ (7) \times 10^{-11}, \tag{2.50}$$

where the error is due to the experimental measure of hadronic e^+e^- annihilation data. The latest value for $a_\mu^{HHO}(lbl)$ was reported in [9]

$$a_\mu^{HHO}(lbl) = +92\ (19) \times 10^{-11}. \tag{2.51}$$

The error is about 20% and it is completely dominated by the model estimates of a numerically subdominant part of the total.

2.2   The Standard Model prediction versus measurement

We now have all the ingredients to derive the SM prediction for a_μ [9]:

$$a_\mu^{SM} = a_\mu^{QED} + a_\mu^{EW} + a_\mu^{HLO} + a_\mu^{HHO}(vp) + a_\mu^{HHO}(lbl) = 116\ 591\ 810\ (43) \times 10^{-11}. \tag{2.52}$$

The latest measurement of the anomalous magnetic moment of negative muons by the experiment E821 at Brookhaven [33] is

$$a_{\mu^-}^{EXP} = 116\ 592\ 689\ (63) \times 10^{-11}, \tag{2.53}$$

The comparison of the SM results with the present experimental average gives the discrepancies

$$(a_\mu^{EXP} - a_\mu^{SM}) = 279\,(76) \times 10^{-11}, \tag{2.54}$$

corresponding to a 3.7σ discrepancy.

The measurement of the muon g-2 by the E821 experiment at Brookhaven is still limited by statistical errors rather than systematic ones. The new E989 Muon g-2 experiment at Fermilab [34] is expected to achieve an unprecedented precision of 0.14 ppm. In addition, a completely new low-energy approach to measuring the g-2 is being developed by the E34 collaboration at J-PARC [35].

Chapter 3

Muon-Electron Scattering

In searching for new physics, low-energy high-precision measurements are complementary to the LHC high-energy frontier. The long standing discrepancy between the experimental value of the muon anomalous magnetic moment and the SM prediction has been considered during these years as one of the most intriguing indications of physics beyond the SM. Nevertheless, the accuracy of the SM prediction, 5×10^{-10}, is limited by strong interaction effects, which cannot be computed perturbatively at low energies. As we saw before, using analyticity and unitarity, the leading-order hadronic contribution to the muon g-2, a_μ^{HLO}, could be computed via a dispersion integral, related to e^+e^- annihilation data at low energy. An alternative evaluation of a_μ^{HLO} can be obtained by lattice QCD calculations [36]. However, current lattice QCD results are not yet competitive with those obtained with the dispersive approach via time-like data.

Recently, a new experiment, MUonE, has been proposed at CERN to determine the leading order hadronic contribution to the muon g-2, measuring the effective electromagnetic coupling in the space-like region via scattering data [37, 38]. A comparison of experimental data with perturbative calculations can be used to extract the hadronic vacuum polarization (HVP) through its contribution to the running of the QED coupling α. The elastic scattering of high energy muons on atomic electrons has been identified as an ideal process for this measurement [39]. The effects of the HVP changes the differential cross section of μe scattering by up to $O(10^{-3})$, depending on the scattering angle of the outgoing electron. In order to reach a determination of the HVP with a precision below one percent, the shape of μe differential cross section must be measured with a systematic uncertainty of the order of 10 ppm or better. An analogous precision is therefore required in the theoretical prediction.

The precision expected at the MUonE experiment also raised the question whether possible new physics (NP) could affect its measurement. The problem was addressed in [40], studying possible NP signals in muon-electron collision at MUonE due to heavy or light mediators (depending on whether their mass is higher or lower than 1 GeV). The former were analysed through an effective field theory approach in a model-independent way, while for the latter different scenarios with light spin-0 and spin-1 bosons were discussed. The authors showed that possible NP effects in muon-electron scattering are

expected to lie below MUonE's sensitivity, hence concluding that it is very unlikely that NP contributions will contaminate MUonE's extraction of the HVP. Another research of NP signals at MUonE was dealt with in [41], where the authors addressed the sensitivity of the experiment to new light scalar or vector mediators, able to explain the muon *g*-2 discrepancy. They concluded that the measurement of the HVP at MUonE is not vulnerable to these NP scenarios. Therefore these two analysis reach similar conclusions when they overlap. These results confirm and reinforce the physics case of the MUonE experiment.

3.1   Theoretical framework

As we have seen in the previous Chapter, with the help of dispersion relation and the optical theorem, the LO hadronic contribution to the muon *g*-2 is given by the formula (2.46). Remembering that $R(s)$ is the ratio of the total $e^+e^- \to hadrons$ and the Born cross section $e^+e^- \to \mu^+\mu^-$, this function in the integrand of (2.46) is highly fluctuating at low energy due to hadronic resonances and threshold effects. Usually the dispersive integral (2.46) is calculated involving the experimental value of $R(s)$ up to a certain value of s and by using perturbative QCD in the high-energy tail [42]. This represents a time-like approach, but an alternative formula can also be exploited [37]: if we exchange the x and the s integration in the equation (2.46), we obtain

$$
\begin{aligned}
a_\mu^{HLO} &= \frac{\alpha}{\pi} \int_0^1 dx (x-1) \bar{\Pi}_{had}[t(x)] \\
&= \frac{\alpha}{\pi} \int_0^1 dx (1-x) \Delta\alpha_{had}[t(x)],
\end{aligned}
\tag{3.1}
$$

where $\Delta\alpha_{had}(t) = -\bar{\Pi}_{had}(t) = -(\Pi_{had}(t) - \Pi_{had}(0))$ is the hadronic contribution to the running of the fine-structure constant, evaluated at

$$
t(x) = \frac{x^2 M^2}{x-1} < 0,
\tag{3.2}
$$

the space-like squared four-momentum transfer, where M is the mass of the muon. In contrast with the integrand function of Eq. (2.46), the integrand in the Eq. (3.1) is smooth and free of resonances.

By measuring the running of α,

$$
\alpha(t) = \frac{\alpha(0)}{1 - \Delta\alpha(t)},
\tag{3.3}
$$

where $t = q^2 < 0$ and $\alpha(0) = \alpha$ is the fine-structure constant in the Thomson limit, the hadronic contribution $\Delta\alpha_{had}(t)$ can be extracted by subtracting from $\Delta\alpha(t)$ the purely leptonic part $\Delta\alpha_\ell(t)$, which can be calculated order-by-order in perturbation theory.

3.2 Kinematics of μe scattering

The proposal of MUonE is to scatter a 150 GeV muon beam on a Beryllium fixed target. In order to obtain sufficient statistics and reduce multiple-scattering effects [43], the target is split into many thin layers. The scattering angles of the electron θ_e and the muon θ_μ (in the lab frame) are measured very precisely.

From an idealised point of view we consider

$$\mu^\pm(p_1)e^-(p_2) \rightarrow \mu^\pm(p_3)e^-(p_4) + X \tag{3.4}$$

where the initial electron is at rest and X stands for any further radiation. Since the energy of the incoming muon is set to $E_1 = 150$ GeV, the center-of-mass energy is fixed as $s = m^2 + M^2 + 2mE_1 \simeq (400 \text{ MeV})^2$, where m and M denote the electron and muon mass, respectively. The momentum transfer t ranges from $t_{min} \simeq -(380 \text{ MeV})^2$ to zero. Therefore, there are two widely different scales entering the process with $m^2 \ll Q^2$, where Q^2 stands for the large scales $M^2 \sim s \sim |t|$. The resulting large logarithms $\log(m^2/Q^2)$ will have to be properly accounted for the theoretical treatment of the process.

In a fixed-target experiment, where the electron is initially at rest, the Mandelstam variables s and t are given by

$$\begin{aligned}
s &= M^2 + m^2 + 2mE_1, \\
t &= 2m^2 - 2mE_4, \\
t_{min} &= -\frac{\lambda(s, M^2, m^2)}{s} \leq t \leq 0.
\end{aligned} \tag{3.5}$$

Here E_1 is the energy of the incident muon, E_4 is the electron recoil energy and

$$\lambda(a,b,c) = a^2 + b^2 + c^2 - 2ab - 2ac - 2bc \tag{3.6}$$

is the Källén function. The third Mandelstam variable u is related to s and t in the usual way as $s + t + u = 2M^2 + 2m^2$. It is also convenient to define the variable x that is related to t as

$$x(t) = \left(1 - \sqrt{1 - \frac{4M^2}{t}}\right)\frac{t}{2M}. \tag{3.7}$$

With $t_{min} \simeq -(380 \text{ GeV})^2$ the range of x is $0 \leq x \lesssim 0.933$ and $x = 0$ corresponds to $t = 0$. Given the incoming muon energy E_1, in a fixed target experiment the variable t is also related to the energy of the scattered electron E_4 or it angle θ_e:

$$E_4 = m\frac{1 + r^2 c_e^2}{1 - r^2 c_e^2}, \qquad \theta_e = \arccos\left(\frac{1}{r}\sqrt{\frac{E_4 - m}{E_4 + m}}\right), \tag{3.8}$$

where

$$r \equiv \frac{\sqrt{E_1^2 - M^2}}{E_1 + m}, \qquad c_e \equiv \cos\theta_e. \tag{3.9}$$

The angle θ_e spans the range $(0 - 31.85)$ mrad for the electron energy in the range $(1 - 139.8)$ GeV.
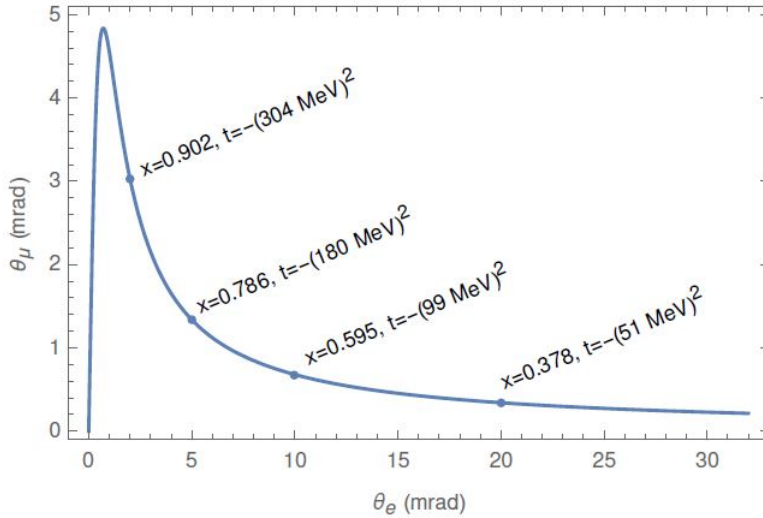
Figure 3.1: The elasticity curve, i.e. the relation between the muon and the electron scattering angles for 150 GeV incident muon beam momentum [44].

The angles of the scattered electron and muon are correlated as shown in Fig. 3.1. This constraint is extremely important to select elastic scattering events, rejecting background events from radiative or inelastic process and to minimize systematic effects in the determination of t. Note that for scattering angle of $(2-3)$ mrad there is an ambiguity between the outgoing electron and muon, as their angles and momenta are similar, to be resolved by means of $\mu - e$ discrimination.

The MUonE experiment is expected to extract $\Delta\alpha_h(t)$ from the shape of the differential μe scattering cross section by a template fit method [39]. The basic idea is that $\Delta\alpha_h(t)$ can be obtained measuring, bin by bin, the ratio N_i/N_n, where N_i is the number of scattering events in a specific t-bin, labelled by the index i, and N_n is the number of events in the normalization t-bin corresponding to $x(t) \sim 0.3$ (for this value of x, $\Delta\alpha_h(t)$ is comparable to the experimental sensitivity expected at MUonE and its error is negligible). Therefore, this measurement will not rely on the absolute knowledge of the luminosity. To extract the leading hadronic correction to the μe scattering cross section in the t-bin i, one can split the theoretical prediction into

$$\sigma_{th,i} = \sigma_i^{(0)}[1 + 2\Delta\alpha_{h,i} + \delta_i + \delta_{NP,i}], \qquad (3.10)$$

where $\sigma_i^{(0)}$ is the LO QED prediction integrated in the t-bin i, $2\Delta\alpha_{h,i}$ is the leading hadronic correction, δ_i is the reminder of the SM corrections, and $\delta_{NP,i}$ is a possible NP contribution. The experimentally measured ratio N_i/N_n can then be equated with the ratio of the theoretical predictions,

$$\frac{N_i}{N_n} = \frac{\sigma_{th,i}}{\sigma_{th,n}} \simeq \frac{\sigma_i^{(0)}}{\sigma_n^0}[1 + 2(\Delta\alpha_{had,i} - \Delta\alpha_{had,n}) + (\delta_i - \delta_n) + (\delta_{NP,i} - \delta_{NP,n})]. \qquad (3.11)$$

As $\Delta\alpha_{had,n}$ is known with a negligible error, if $(\delta_i - \delta_n)$ is computed with sufficient precision,

one can extract

$$2\Delta\alpha_{had,i} + (\delta_{NP,i} - \delta_{NP,n}), \tag{3.12}$$

bin by bin, from N_i/N_n. Equation (3.11) shows that the impact of the SM corrections on this extractions can only be established after subtracting their value in the normalization region, and that, as we underlined before, the MUonE experiment will not be sensitive to a NP signal constant in t relative to the LO QED one, i.e. such that $\delta_{NP,i} = \delta_{NP,n}$ [40]. In any case, as already discussed, possible NP effects in muon-electron scattering are expected to lie below MUonE's sensitivity.

3.3 Fixed-order calculations

In order to achieve our goal of a relative accuracy of 10 ppm, we need to calculate μe scattering at least up to NNLO in the perturbative expansion in the electromagnetic coupling $\alpha \sim 1/137$.

3.3.1 Leading order

The leading order SM prediction for the differential cross section of the μe elastic scattering is characterized by two diagrams with a t-channel exchange of a photon and a Z boson.
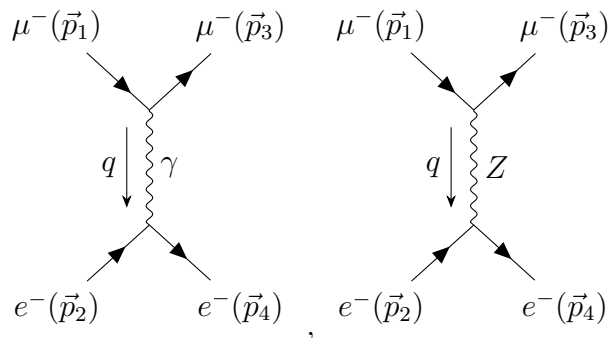
It is precisely this feature that makes this process ideal to extract the HVP. Indeed, the dominant contribution of the HVP is simply given by the insertion of the hadronic vacuum polarization Π_{had} in the photon propagator.
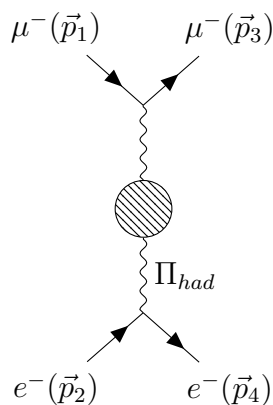
Therefore, calling M_γ and M_Z the Feynman matrix elements originating from the two diagrams above, the LO unpolarized amplitude $\mathcal{X}^{LO}$ may be written as

$$\mathcal{X}^{LO} = \frac{1}{4} \sum_{spins} |M_\gamma + M_Z|^2 = \mathcal{X}_\gamma + \mathcal{X}_Z + \mathcal{X}_{\gamma Z}, \tag{3.13}$$

where the 1/4 factor is related to the fact that we are averaging over the initial spins of two leptons. The contributions due to the exchange of a Z boson are strongly suppressed because of its large mass M_Z. However, the interference between the Z-boson and photon-exchange diagrams is suppressed with respect to the LO QED contribution only by $Q^2/M_Z^2 \simeq 10^{-5}$. Hence, this effect is relevant and needs to be taken into account in the calculation.

The unpolarized Feynman amplitude related to the exchange of a photon is easily computable via the Feynman rules, yielding

$$M_\gamma = \frac{ie^2}{t} \bar{u}(p_3)\gamma^\mu u(p_1)\bar{u}(p_4)\gamma_\mu u(p2) \tag{3.14}$$

$$\mathcal{X}_\gamma = \frac{1}{4} \sum_{spins} |M_\gamma|^2 = \frac{64\pi^2\alpha^2}{t^2} f(s,t), \tag{3.15}$$

where

$$f(s,t) = (m^2 + M^2 - s)^2 + st + \frac{t^2}{2}. \tag{3.16}$$

Consequently, the differential cross section of the μe elastic scattering with a γ exchange is

$$\frac{d\sigma_0}{dt} = \frac{\mathcal{X}_\gamma}{16\pi\lambda(s,M^2,m^2)} = \frac{4\pi\alpha^2 f(s,t)}{t^2 \lambda(s,M^2,m^2)}. \tag{3.17}$$

The unpolarized Feynman amplitude related to the interference between the Z-boson and photon-exchange diagrams is easily computable via the Feynman rules. Remember that we consider this LO correction induced by the exchange of a Z boson for $|t| \ll M_Z^2$.

$$
\begin{aligned}
M_Z &= \left(\frac{-ig}{4\cos\theta_w}\right)^2 \bar{u}(p_3)\gamma_\mu(g_V - g_A\gamma^5)u(p_1)\frac{i}{t^2 - M_Z^2}\left(-g^{\mu\nu} + \frac{k^\mu k^\nu}{M_Z^2}\right)\bar{u}(p_4)\gamma_\nu(g_V - g_A\gamma^5)u(p_2) \\
&= \frac{-iG_F}{2\sqrt{2}}\bar{u}(p_3)\gamma_\mu(g_V - g_A\gamma^5)u(p_1)\bar{u}(p_4)\gamma^\mu(g_V - g_A\gamma^5)u(p_2)
\end{aligned}
\tag{3.18}
$$

where the Z-boson propagator reduces to $-1/M_Z^2$ in the low energy limit, G_F is the Fermi constant, related to the charged vector boson mass M_W or M_Z and $\cos\theta_w$ by

$$\frac{G_F}{\sqrt{2}} = \frac{g^2}{8M_W^2} = \frac{g^2}{8M_Z^2\cos^2\theta_w}, \tag{3.19}$$

and finally g_V and g_A are the vector and axial couplings, defined via the weak isospin third-component I_w^3 and the lepton charge Q:

$$
\begin{aligned}
g_V &= 2I_w^3 - 4Q\sin^2\theta_w \\
g_A &= 2I_w^3
\end{aligned}
\tag{3.20}
$$

At this point we have all the tools to evaluate the interference term, obtaining

$$\mathcal{X}_{\gamma,Z} \equiv \delta_Z = \frac{1}{4}\sum_{spins} 2\mathrm{Re}[(M_\gamma)^* M_Z] = -\frac{G_F t}{4\pi\alpha\sqrt{2}}\left[a_\theta^2 - \frac{(s-u)t}{2f(s,t)}\right], \qquad (3.21)$$

where $a_\theta = 4s_\theta^2 - 1$, $s_\theta^2 \approx 0.22$ is the squared sine of the weak mixing angle. For the values of s and t considered in the MUonE experiment, the Z boson correction δ_Z is positive[1], and $0 < |\delta_Z| < 1.5 \times 10^{-5}$, with $\delta_Z = 0$ for $t = 0$.

By adding together the results (3.15) and (3.21), we obtain the LO SM prediction for the μe differential cross section

$$\frac{d\sigma_{LO}}{dt} = \frac{d\sigma_0}{dt}(1 + \delta_Z). \qquad (3.22)$$

As the MUonE experiment is expected to measure the shape of the differential cross section with a relative uncertainty of $O(10^{-5})$ or better close to the endpoint $t = t_{min}$, the maximum Z boson effect is expected to be comparable with the experimental uncertainty. The tiny correction to (3.22) induced by the exchange of a Higgs boson of mass M_H is further suppressed by a factor of $O(m^2 M^2 / t M_H^2)$ with respect to δ_Z and is therefore negligible.

3.3.2 Next-to-leading order

Going to next-to-leading order (NLO), the separately divergent real and virtual contributions have to be combined in order to obtain a physical result. NLO QED corrections to (3.17) were computed long time ago [45]-[51], with various approximations, and revisited in [52]. Recently, a fully differential NLO code [53] has been used to perform a detailed phenomenological study, taking into account the full m dependence. Therefore, we focus on these NLO corrections, verifying their consistency with the results in literature.

At NLO there are three types of diagrams contributing to the cross section of the process
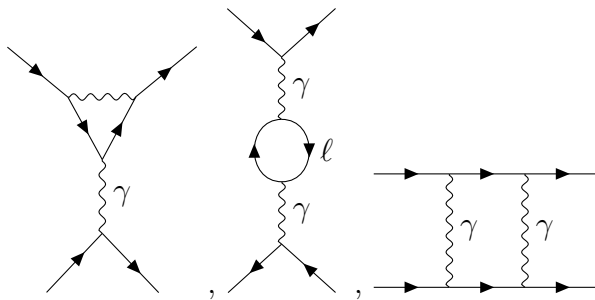
The virtual corrections are computed considering the interference between these diagrams and the LO one with the exchange of a photon:

$$\mathcal{X}^{NLO} = \frac{1}{4}\sum_{spins} 2\mathrm{Re}[(M_\gamma)^* M_{NLO}] \qquad (3.23)$$

---

[1]Because we are considering muons μ^-, otherwise if we consider the anti-muon μ^+, the correction δ_Z is negative.

where M_{NLO} is the sum of the amplitudes originating from the two-, three-, four-point one-loop diagrams. The NLO leptonic correction to Eq. (3.22) are given by

$$\frac{d\sigma_{NLO,\ell}}{dt} = 2\Delta\alpha_\ell(t)\frac{d\sigma_0}{dt}. \tag{3.24}$$

All the standard QED renormalization calculations were carried out using *Mathematica* and *FeynCalc* [54]. In particular, the latter decomposes the loop integral into a sum of tensor integral by the function OneLoop; then it reduces the results to Passarino-Veltman (PV) scalar integrals via PaVeReduce.

A.   Vacuum polarization

The renormalization at one-loop of the photon field and electric charge implies the replacements

$$e_0 \qquad \longrightarrow \qquad e + ie^2\Pi^{\mu\nu}(k^2) + i(Z_A - 1)(k^\mu k^\nu - k^2\eta^{\mu\nu}) \tag{3.25}$$

where we have called $ie^2\Pi^{\mu\nu}(k^2)$ our to-be-computed loop integral and it characterizes by the Lorentz structure

$$ie^2\Pi^{\mu\nu} = ie^2(k^\mu k^\nu - g^{\mu\nu}k^2)\Pi(k) \tag{3.26}$$

We can focus only on the bubble, truncating the external legs and using the Feynman rules to write the amplitude of $\Pi^{\mu\nu}$ in d dimension

$$ie^2\Pi^{\mu\nu} = (-ie\mu^{\frac{\epsilon}{2}})^2(-1)\int \frac{d^d k}{(2\pi)^d}\frac{\text{Tr}[\gamma^\mu i(\slashed{k}+m)\gamma^\nu i(\slashed{k}+\slashed{q}+m)]}{(k^2-m^2)((k+q)^2-m^2)} \tag{3.27}$$

where $\epsilon = 4 - d$, $q = p_3 - p_1$, μ is the 't Hooft dimensional parameter and k is the loop momentum. The contributions with a muon or a tau bubble could be obtained through the substitutions $m \to M$ and $m \to M_\tau$, respectively. Since the vacuum polarization diagram is linearly UV divergent and in remormalized perturbation theory, in order to obtain a physical finite result, it is necessary to introduce a counterterm to absorb that divergence

$$\delta_A(m_i) = \frac{e^2}{12\pi^2}\left[\frac{1}{\epsilon} - \gamma + \log(4\pi\mu^2)\right] \tag{3.28}$$

where γ is the Euler constant. Therefore

$$Z_A = 1 - \delta_A(m_i). \tag{3.29}$$

Only after subtracting the UV divergence, we are allowed to take the limit $d \to 4$.

The contribution of order $O(\alpha^3)$ to the differential cross section from self energy diagrams may be addressed as

$$\mathcal{X}_2^{NLO} = \frac{1}{2}\text{Re}[(M_\gamma)^* \times \sum_{e,\mu,\tau}(M_\Pi)] \qquad (3.30)$$

where we have to take the sum over electron, muon and tau bubble.

Through the substitution of Eq. (3.27) for the photon propagator in the LO amplitude (3.15), we obtain

$$\mathcal{X}_2^{NLO} = \text{Re}[\frac{64\pi\alpha^3}{9t^3}2f(s,t)\sum_{m_i}(-3(2m_i+t)fb_0(t,m_i^2,m_i^2)+6m_i^2fb_0(0,m_i^2,m_i^2)-6t\log m_i+t)] \qquad (3.31)$$

where $m_i = m, M, M_\tau$, and fb_0 is the finite part of the two-point PV integrals, indeed

$$B_0(k,m_1,m_2) = \frac{2}{\epsilon} - \gamma + \log(4\pi\mu^2) + fb_0(k,m_1,m_2). \qquad (3.32)$$

B.   Vertex renormalization

In the previous Chapter we have seen the Lorentz structure of the QED vertex by means of a Lorentz decomposition (2.14). After that, we have introduced our renormalized vertex (2.15). As we have done for the vacuum polarization, we work in d dimension and through the Feynman rules we obtain the following amplitude
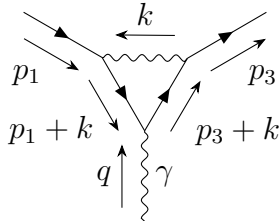
$$ie^2\bar{u}(p_3)\Gamma^\mu u(p_1) = (e^2\mu^{\frac{\epsilon}{2}})^3 \int \frac{d^dk}{(2\pi)^d} \frac{\bar{u}(p_3)\gamma^\nu(\slashed{p}_1 + \slashed{k} + M)\gamma^\mu(\slashed{p}_3 + \slashed{k} + M)\gamma_\nu u(p_1)}{[(p_1+k)^2 - M^2][(p_3+k)^2 - M^2][k^2 - \lambda^2]} \qquad (3.33)$$

where k is the loop momentum and λ is a fictitious mass for the photon. Indeed the vertex diagram is not only UV divergent, but also IR, therefore we introduce the photon mass λ in order to regularize the IR divergences. We can obtain the contribution of the electron triangle performing the substitutions $M \to m$, $p_1 \to p_2$ and $p_3 \to p_4$.

Since we have already regularized the IR divergences and the vertex diagram is logarithmically UV divergent, we have to introduce a counterterm to absorb the divergence and to obtain a physical finite result:

$$\delta_V(m_i) = \frac{e^2}{16\pi^2}\left(\frac{2}{\epsilon} - \gamma + \log(4\pi\mu^2) + 4\log\lambda - 6\log m_i + 5\right) \qquad (3.34)$$

where

$$Z_V = 1 - \delta_V(m_i). \qquad (3.35)$$

Only at this stage, after subtracting the UV divergences, we are allowed to take the limit $d \to 4$, while we have first to sum the soft LO Bremsstrahlung contribution, before taking $\lambda \to 0$ (see section 3.3.2.4).

The contribution of order $O(\alpha^3)$ to the differential cross section from vertex diagrams may be adressed as

$$\mathcal{X}_3^{NLO} = \frac{1}{2} \text{Re}[(M_\gamma)^* \times \sum_{e,\mu} M_\Gamma] \tag{3.36}$$

where we have to take the sum over the muon and the electron vertex contributions. Through the substitution of Eq. (3.33) for the vertex in the LO amplitude (3.22), we obtain

$$\mathcal{X}_{3,\mu}^{NLO} = \frac{8\pi\alpha^3}{t^2(4M^2 - t)} [2f(s,t)(2(-6M^2 t + 8M^4 + t^2)C_0(M^2, M^2, t, M^2, \lambda^2, M^2)+$$
$$+ 4(3M^2 - t)fb_0(0, M^2, M^2) + (3t - 8M^2)fb_0(t, M^2, M^2) + 4\log\lambda(t - 4M^2)+$$
$$+ 6(4M^2 - t)\log M - 3t) - 8M^2 t(2m^2 + t)(-fb_0(t, M^2, M^2) + fb_0(0, M^2, M^2) + 3)]. \tag{3.37}$$

Performing the substitution $M \to m$, we obtain the contribution of $\mathcal{X}_{3,e}^{NLO}$.

C. Box diagrams

Considering the following planar and crossed box diagrams,
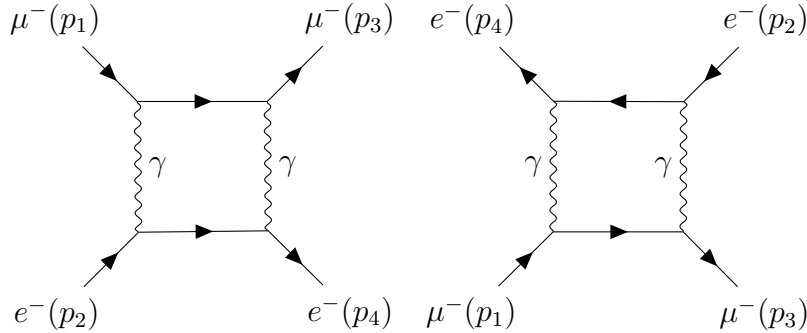
one may note that, by making use of the Feynman rules and dimensional regularization, these diagrams are not UV divergent. In particular, inverting for example the arrows on the muon line, the crossed diagrams turns out to be identical to the planar one, if an overall minus sign is added in front and the following substitution is done $u = 2M^2 + 2m^2 - s - t \to s$. Therefore, we can check our calculations through a comparison between the direct diagram and the crossed one.

At this point we can write the following amplitude in d dimension:

$$B_p = e^4 \int \frac{d^d k}{(2\pi)^d} \frac{\bar{u}(p_4)\gamma^\mu(m - \slashed{k})\gamma^\nu u(p_2)\bar{u}(p_3)\gamma_\mu(\slashed{k} + \slashed{p}_3 + \slashed{p}_4 + M)\gamma_\nu u(p_1)}{((k + p_3 + p_4)^2 - M^2)((k + p_4)^2 - \lambda^2)((k + p_2)^2 - \lambda^2)(k^2 - m^2)}, \tag{3.38}$$

where k is the loop momentum. We can derive the contribution from the crossed box B_c via the substitutions $p_1 \to -p_3$, $p_3 \to -p_1$ applied to the whole expression, leaving

the spinors unchanged. We also remind to the reader that these contributions are not UV divergent and we have first to sum the LO soft Bremsstrahlung contribution, before taking $\lambda \to 0$ in both cases, like what we have done for the vertex correction (see section 3.3.2.4).

The unpolarized $O(\alpha^3)$ contribution from box diagrams may be addressed as

$$\mathcal{X}_4^{NLO} = \frac{1}{2}\text{Re}[(M_\gamma)^* \times (M_{bp} + M_{bc})] \tag{3.39}$$

In this case, in order to simplify the computation, we have exploit the fact that the box diagrams are ultraviolet finite. Indeed, in order to use the Dirac equation and contract the Lorentz indices, we first contracted the amplitude (3.38) with the LO one (3.15), then we solve the loop integral in terms of PV functions. Obtaining,

$$
\begin{aligned}
\mathcal{X}_4^{NLO} = 16\pi\alpha^3 \Big[&c_0 + c_1 f b_0(0, m^2, m^2) + c_2 f b_0(0, M^2, M^2) + c_3 f b_0(s, m^2, M^2) + \\
&+ c_4 f b_0(2M^2 + 2m^2 - s - t, m^2, M^2) + c_5 f b_0(t, 0, 0) + c_6 C_0(m^2, m^2, t, 0, m^2, 0) + \\
&+ c_7 C_0(M^2, M^2, t, 0, M^2, 0) + c_8 C_0(m^2, M^2, s, m^2, \lambda^2, M^2) + \\
&+ c_9 C_0(m^2, M^2, 2m^2 + 2M^2 - s - t, m^2, \lambda^2, M^2) + \\
&+ c_{10} D_0(m^2, m^2, M^2, M^2, t, s, \lambda^2, m^2, \lambda^2, M^2) + \\
&+ c_{11} D_0(m^2, m^2, M^2, M^2, t, 2M^2 + 2m^2 - s - t, m^2, \lambda^2, M^2) \Big]
\end{aligned}
\tag{3.40}
$$

where

$$
\begin{aligned}
c_0 = &\frac{8(m^2 - M^2)^2 - 8(m^2 + M^2)s}{m^4 + (M^2 - s)^2 - 2m^2(M^2 + s)} + \frac{4(m + M)^2}{(m - M)^2 - s - t} + \frac{4(m - M)^2}{(m + M)^2 - s - t} + \\
&+ \frac{16(m^2 + M^2 - s)}{t} + \frac{8(m^2 - M^2 + s)}{-4m^2 + t} - \frac{8(m^2 - M^2 - s)}{-4M^2 + t},
\end{aligned}
\tag{3.41}
$$

$$
\begin{aligned}
c_1 = &\frac{4m^2(m^2 - M^2 - s)}{m^4 + (M^2 - s)^2 - 2m^2(M^2 + s)} + \frac{2m(m + M)}{(m - M)^2 - s - t} + \frac{2m(m - M)}{(m + M)^2 - s - t} + \\
&+ \frac{4(m^2 + M^2 - s)}{t} + \frac{4(m^2 - M^2 + s)}{-4m^2 + t},
\end{aligned}
\tag{3.42}
$$

$$
\begin{aligned}
c_2 = &\frac{4M^2(-m^2 + M^2 - s)}{m^4 + (M^2 - s)^2 - 2m^2(M^2 + s)} + \frac{2M(m + M)}{(m - M)^2 - s - t} + \frac{2M(-m + M)}{(m + M)^2 - s - t} + \\
&+ \frac{4(m^2 + M^2 - s)}{t} + \frac{4(-m^2 + M^2 + s)}{-4M^2 + t},
\end{aligned}
\tag{3.43}
$$

$$
c_3 = -\frac{2(m^6 + (M^2 - s)^3 + (M^4 - s^2)t + m^4(-M^2 - 3s + t) - m^2(M^4 - 3s^2 + 2M^2(s + t)))}{((m - M)^2 - s)((m + M)^2 - s)t},
\tag{3.44}
$$

$$c_4 = -\frac{2(m^2 + M^2 - s)}{t} - \frac{2(m - M)^2}{(m + M)^2 - s - t} - \frac{2(m + M)^2}{(m - M)^2 - s - t}, \tag{3.45}$$

$$c_5 = \frac{2(4mM - t)(2(m^2 + M^2 - s) - t)(4mM + t)}{(4m^2 - t)t(-4M^2 + t)}, \tag{3.46}$$

$$c_6 = \frac{2(2(m^2 + M^2 - s) - t)(8m^4 - 8m^2 t + t^2)}{(4m^2 - t)t}, \tag{3.47}$$

$$c_7 = \frac{2(2(m^2 + M^2 - s) - t)(8M^4 - 8M^2 t + t^2)}{(4M^2 - t)t}, \tag{3.48}$$

$$c_8 = \frac{2(m^2 + M^2 - s)(2s + t)}{t}, \tag{3.49}$$

$$c_9 = \frac{2(4m^2 + 4M^2 - 2s - t)(m^2 + M^2 - s - t)}{t}, \tag{3.50}$$

$$c_{10} = \frac{(m^2 + M^2 - s)(-4(m^2 + M^2 - s)^2 - 2st - t^2)}{t}, \tag{3.51}$$

$$c_{11} = -\frac{(m^2 + M^2 - s - t)(4(m^2 + M^2 - s)^2 - 4(m^2 + M^2)t + 6st + 3t^2)}{t}. \tag{3.52}$$

D.   Soft Bremsstrahlung contribution

At this point we have obtained the NLO virtual contribution to muon-electron cross section, which is UV finite. Keeping a finite m complicates the computation of the virtual corrections. However, it serves as a regulator for collinear singularities which are replaced by $\log(m^2/Q^2)^2$ and only soft singularities are left, regularised by the introduction of a fictitious photon mass λ.

We consider soft photon emission both in the initial and in the final state, only when the emitted photon has an energy less than ω, where ω is the threshold of the experimental setup. The cross section will be IR finite if soft Bremsstrahlung diagrams are summed to the virtual contribution.

Consider the process in which one photon is radiated during the μe scattering

---
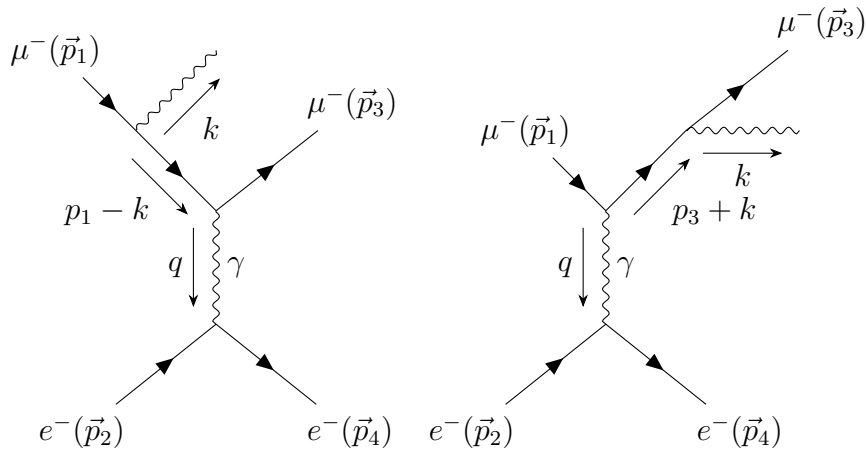
[2]We remember that Q^2 stands for large scales, like $M^2 \sim s \sim |t|$.
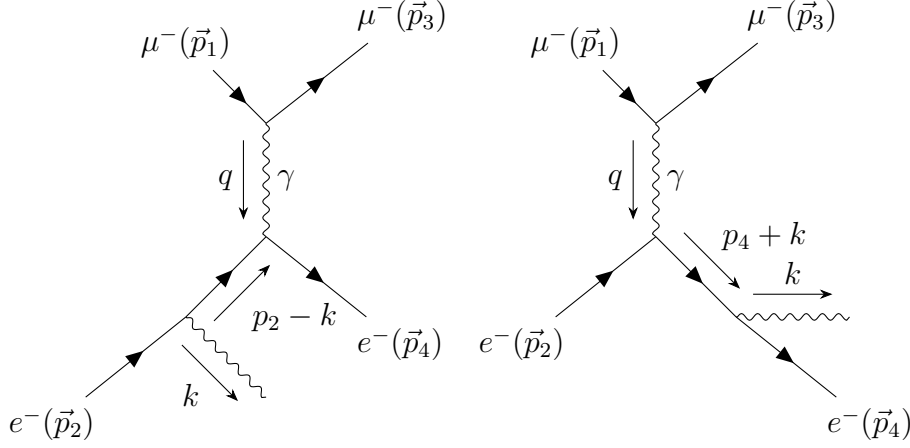
Being $k = (k^0, \mathbf{k})$ the soft photon four-momentum. For example, let's focus on the first diagram, using the Feynman rules we obtain

$$\mathcal{M}_1 = \frac{ie^3}{t} \bar{u}(p_4)\gamma^\mu u(p_2)\bar{u}(p_3)\gamma_\mu \frac{(-\not{k} + \not{p}_1 + M)}{(p_1 - k)^2 - M^2}\not{\epsilon}^*(k)u(p_1). \tag{3.53}$$

Being the photon soft, we may neglect $\not{k}$ with respect to $\not{p}_1$ and using the Clifford algebra $\{\gamma^\mu, \gamma^\nu\} = 2g^{\mu\nu}$ and the Dirac equation, we find

$$\mathcal{M}_1 = \frac{ie^3}{t} [\bar{u}(p_4)\gamma^\mu u(p_2)\bar{u}(p_3)\gamma_\mu u(p_1)]\frac{p_1 \cdot \epsilon}{-p_1 \cdot k}. \tag{3.54}$$

At this point, we can obtain the unpolarized squared amplitude taking the absolute square of $\mathcal{M}_1$, remembering that the sum over polarizations yields:

$$\sum_{pol} \epsilon^\alpha \epsilon^\beta = -g^{\alpha\beta} \tag{3.55}$$

In particular, we cal also neglect the k in the four-momentum conservation δ, due to the fact that the recoil of the fermion by the emitted photon is neglected.

Clearly, the other three diagrams give similar contributions through the substitutions $(p_1 \to p_3, k \to -k)$, $p_1 \to p_2$ and $(p_1 \to p_4, k \to -k)$.

The squared amplitude for our process is easy to express in terms of the LO contribution; just inserting an additional phase-space integration for the photon variable k, we have:

$$\mathcal{X}_{LO}^\omega = -\mathcal{X}_\gamma e^2 \int^{k^0 < \omega} \frac{d^3k}{(2\pi)^3 2k^0} |\mathcal{E}(p_1, p_2, p_3, p_4, k)|^2, \tag{3.56}$$

where

$$\mathcal{E}(p_1, p_2, p_3, p_4, k) = -\frac{p_1}{p_1 \cdot k} + \frac{p_3}{p_3 \cdot k} - \frac{p_2}{p_2 \cdot k} + \frac{p_4}{p_4 \cdot k}. \tag{3.57}$$

In computing the soft Bremsstrahlung one encounters an integral that is essentially a phase-space integral for photons with energy less than ω. We followed the approach proposed by 't Hooft and Veltman in [55].

A generalization of the integral is

$$\mathcal{I}(p_i, p_j) = \int^{k^0 < \omega} \frac{d^3 k}{k^0} \frac{1}{(p_i \cdot k)(p_j \cdot k)}. \tag{3.58}$$

Then in the LAB frame,

$$\begin{aligned}
\mathcal{X}_{LO}^{\omega} = \frac{16\alpha^3}{t^2} f(s,t)[&2(m^2 + M^2 - s)\mathcal{I}(p_1, p_2) + (2M^2 - t)\mathcal{I}(p_1, p_3)+ \\
+ &(2m^2 - t)\mathcal{I}(p_2, p_4) - 2M^2\mathcal{I}(p_1, p_1) - 2m^2\mathcal{I}(p_2, p_2)+ \\
+ &2(m^2 + M^2 - u)\mathcal{I}(p_2, p_3)].
\end{aligned} \tag{3.59}$$

The integrals with $p_i = p_j$ yield a direct calculation, while in the other cases the procedure is more articulate and we follow the results of 't Hooft and Veltman in [55].

In this section we keep the implicit form of the integrals, while their evaluation is quoted in Appendix B.

Finally, taking the sum between one-loop virtual contributions and real soft LO Bremsstrahlung diagrams, we verify the cancellation of IR divergences (i.e. the cancellation of the coefficients of $\log \lambda$ terms) in the following expressions:

- Muon Vertex Correction

$$\begin{aligned}
\text{Re}[&\frac{32\pi\alpha^3}{t^2(4M^2 - t)} f(s,t)(2(8M^4 - 6M^2 t + t^2)C_0(M^2, M^2, t, M^2\lambda^2, M^2)- \\
&- 4(4M^2 - t)\log\lambda) + \frac{16\alpha^3}{t^2} f(s,t)((2M^2 - t)\mathcal{I}(p_1, p_3) - 2M^2\mathcal{I}(p_1, p_1))],
\end{aligned} \tag{3.60}$$

- Electron Vertex Correction

$$\begin{aligned}
\text{Re}[&\frac{32\pi\alpha^3}{t^2(4m^2 - t)} f(s,t)(2(8m^4 - 6m^2 t + t^2)C_0(m^2, m^2, t, m^2\lambda^2, m^2)- \\
&- 4(4m^2 - t)\log\lambda) + \frac{16\alpha^3}{t^2} f(s,t)((2m^2 - t)\mathcal{I}(p_2, p_4) - 2m^2\mathcal{I}(p_2, p_2))],
\end{aligned} \tag{3.61}$$

- Planar Box

$$\begin{aligned}
\text{Re}[&16\pi\alpha^3(c_8 C_0(m^2, M^2, s, m^2, \lambda^2, M^2) + c_{10} D_0(m^2, m^2, M^2, M^2, t, s, \lambda^2, m^2, \lambda^2, M^2))+ \\
&+ \frac{16\alpha^3}{t^2} f(s,t)(2(m^2 + M^2 - s)\mathcal{I}(p_1, p_2))],
\end{aligned}$$

$$\tag{3.62}$$

- Crossed Box

$$\begin{aligned}
\text{Re}[&16\pi\alpha^3(c_9 C_0(m^2, M^2, u, m^2, \lambda^2, M^2) + c_{11} D_0(m^2, m^2, M^2, M^2, t, u, \lambda^2, m^2, \lambda^2, M^2))+ \\
&+ \frac{16\alpha^3}{t^2} f(s,t)(2(m^2 + M^2 - u)\mathcal{I}(p_2, p_3))],
\end{aligned}$$

$$\tag{3.63}$$

Only at this point, we can safely take the limit $\lambda \to 0$. In particular, we remember that $C_0(m^2, m^2, t, 0, m^2, 0)$ and $C_0(M^2, M^2, t, 0, M^2, 0)$, showing up in the box contributions, are already IR finite, differently from all the other three- and four-point Passarino-Veltman functions [56].

Actually, the MUonE experiment is not expected to detect photons in the final state. Therefore, the theoretical needed result to match MUonE's measurements should include also the hard Bremsstrahlung contributions to obtain a physical result.

Chapter 4

# Muon-Electron Scattering at NNLO: The Leptonic Corrections

The QED corrections at next-to-next-to-leading order (NNLO), crucial to interpret the high precision data of future experiments like MUonE, are not yet known, although some of the two-loop corrections which were computed for Bhabha scattering in QED [57]-[59] and for $t\bar{t}$ production in QCD [60, 61] can be applied to μe scattering as well. A first step towards the calculation of the full NNLO QED corrections to μe scattering was taken in Refs. [62]-[64], where the master integrals for the two-loop planar and non-planar four point Feynman diagrams were computed. These integrals were calculated setting the electron mass to zero, while retaining full dependence on the muon one. The extraction of the leading electron mass effects from the massless muon-electron scattering amplitudes has been recently addressed in [65]. Very recently, two independent Monte Carlo tools have been built including the partial (gauge invariant) subsets of the NNLO QED corrections due to electron and muon radiation [66, 67]. Additionally, also an approximation of the full NNLO photonic corrections has been implemented, which already provides the complete general structure of the NNLO QED Monte Carlo code, to be used as soon as the missing matrix elements for NNLO virtual corrections will become available.

In this chapter we will study the leptonic NNLO QED corrections to μe scattering, taking the full m dependence. The leptonic NNLO QED contributions arise from two-loop QED diagrams with leptonic vacuum polarization insertions in the photon propagator. These corrections, of order $O(\alpha^4)$, can be split into five different classes of diagrams. The first four classes contain factorizable contributions, i.e. amplitudes that can be written as the product of a QED amplitude times the leptonic vacuum polarization function $\Pi_\ell(q^2)$ evaluated at some q^2 fixed by the external kinematics. They are:
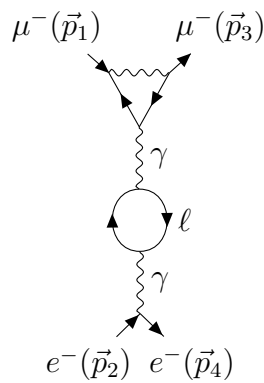
- Class 0: QED tree-level diagram with the insertion of a "bubble" of two-loop leptonic vacuum polarization.

$$\mu^-(\vec{p}_1) \quad \mu^-(\vec{p}_3)$$
$$\gamma$$
$$\gamma \qquad \ell$$
$$\gamma$$
$$e^-(\vec{p}_4) \quad e^-(\vec{p}_2)$$
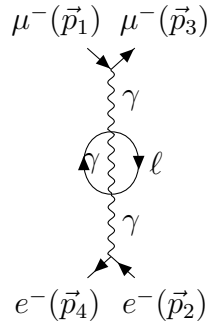
- Class I: tree-level diagrams in combination with one or two leptonic vacuum polarization insertions.

$$\mu^-(\vec{p}_3) \, \mu^-(\vec{p}_1)$$
$$\gamma$$
$$\ell$$
$$\gamma$$
$$\ell$$
$$\gamma$$
$$e^-(\vec{p}_4) \, e^-(\vec{p}_2)$$
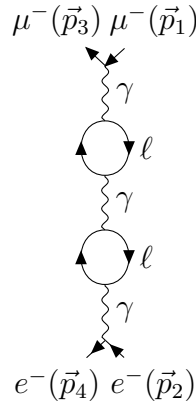
- Class II: QED one-loop diagrams in combination with one leptonic vacuum polarization insertion in the t-channel photon.

$$\mu^-(\vec{p}_1) \qquad \mu^-(\vec{p}_3)$$
$$\gamma$$
$$\ell$$
$$\gamma$$
$$e^-(\vec{p}_2) \quad e^-(\vec{p}_4)$$

Their contribution to the differential cross section is proportional to $\Pi_\ell(t)$ and a combination of one-loop QED corrections to μe scattering.

- Class III: real photon emission diagrams with a leptonic vacuum polarization insertion in the t-channel photon.
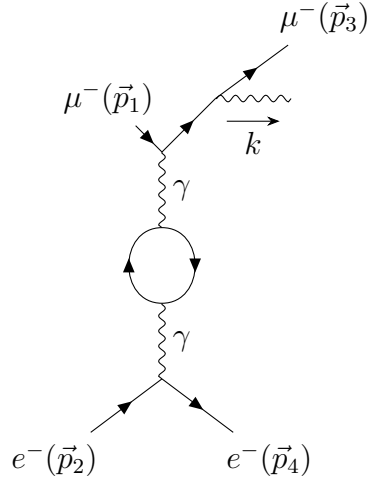
Moreover a fourth class of non-factorizable diagrams must be considered:

- Class IV: one-loop QED amplitudes with a leptonic vacuum polarization insertion in the loop. They can be further subdivided into vertex and box corrections.
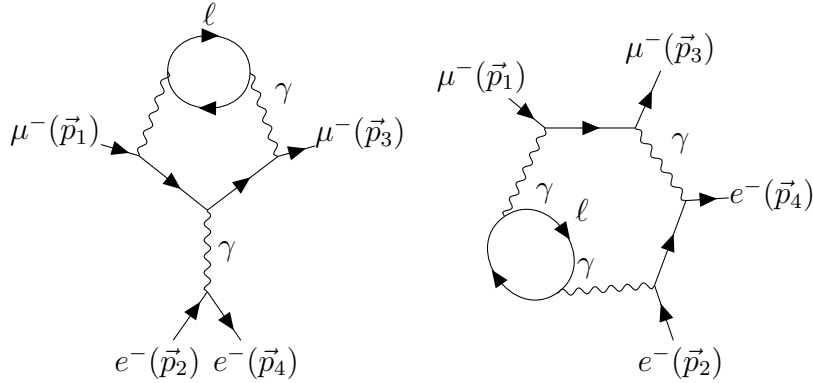
In particular, the evaluation of the leptonic NNLO QED corrections is complicated by the presence of these non-factorizable two-loop diagrams. We will present their calculation using the dispersive approach. This approach is analogous to that employed for the recent determination of the NNLO hadronic corrections addressed in Ref. [68]. Moreover, it was shown in [69] that these NNLO hadronic corrections can also be calculated by employing the hadronic vacuum polarization in the space-like region, taking advantage of the hyperspherical integration method, without using time-like data.

4.1   Dispersion relations and the vacuum polarization

Dispersion relations play an important role for taking into account the photon propagator contributions. Let's consider a complex function of the Mandelstam variable s, $f(s)$, with
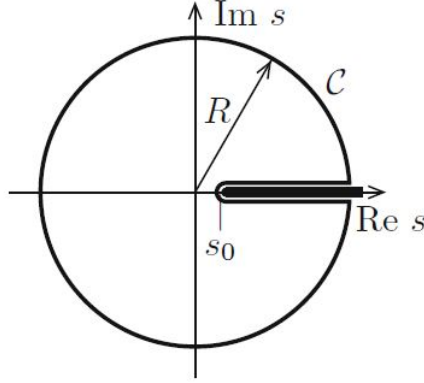
Figure 4.1: Analyticity domain and Cauchy contour $\mathcal{C}$ for the function $f(s)$

a branch cut along the real positive axis in the s-plane for $s > s_0$. Then we may write $f(s)$ in terms of a Cauchy integral

$$f(s) = \frac{1}{2\pi i} \oint_{\mathcal{C}} \frac{ds' f(s')}{s' - s}, \tag{4.1}$$

for the contour $\mathcal{C}$ shown in Figure. 4.1.

Since $f(s)$ may be defined for complex s in the upper half s-plane, the Schwartz reflection principle allows us to extend the domain of $f(s)$ to the lower half s-plane by $f(s^*) = f^*(s)$. Therefore the contribution along the cut may be written as

$$\lim_{\epsilon \to 0} \left(f(s + i\epsilon) - f(s - i\epsilon) \right) = 2i \text{Im}[f(s)] \tag{4.2}$$

and we may rewrite (4.1) as

$$f(s) = \frac{1}{2\pi i} \int_{s_0}^{\infty} \frac{ds' 2i \text{Im}[f(s)]}{s' - s} + \frac{1}{2\pi i} \int_{\mathcal{C}_{\infty}} \frac{ds' f(s')}{s' - s}. \tag{4.3}$$

If the contribution from $\mathcal{C}_{\infty}$ vanishes in the limit $R \to \infty$, than $f(s)$ falls off sufficiently rapidly in this limit and the latter equation yields a dispersion relation (DR) for $f(s)$:

$$f(s) = \frac{1}{\pi} \int_{s_0}^{\infty} \frac{ds' f(s')}{s' - s}. \tag{4.4}$$

If the contribution from the circle $\mathcal{C}_{\infty}$ does not vanish (so the fall off condition is not satisfied), we may subtract $f(a)$ from $f(s)$, for any a in the domain of $f(s)$:

$$f(s) - f(a) = \frac{s - a}{\pi} \int_{s_0}^{\infty} \frac{ds' \text{Im}[f(s')]}{(s' - s)(s' - a)} \tag{4.5}$$

this latter equation is called subtracted dispersion relation (SDR), which exhibits one additional power of s' in the denominator and hence improves the damping of the integrand at large s' by one additional power.

To evaluate the leptonic NNLO QED corrections to μe scattering, let us consider the SM vacuum polarization tensor with four-momentum q. In QED, the photon self-energy, obtained from the photon propagator by the amputation of the external photon lines, may be described as the vacuum expectation value of the time ordered product of two electromagnetic currents

$$
\begin{aligned}
i\Pi^{\mu\nu}(q) &= i\Pi(q^2)(g^{\mu\nu}q^2 - q^\mu q^\nu) \\
&= \int d^4x e^{iqx}\langle 0|T\{j_{em}^\mu(x)j_{em}^\nu(0)\}|0\rangle,
\end{aligned}
\tag{4.6}
$$

where $j_{em}^\mu(x) = \sum_f Q_f \bar{\psi}_f(x)\gamma^\mu\psi_f(x)$ is the electromagnetic current and the sum runs over fermions with charges Q_f. The transverse part of the full photon propagator is

$$
\frac{-ig^{\mu\nu}}{q^2[1 + \Pi(q^2)]} = \frac{-ig^{\mu\nu}}{q^2}[1 - \Pi(q^2) + \Pi^2(q^2)]
\tag{4.7}
$$

where $\Pi(q^2)$ is the renormalized vacuum polarization function satisfying the condition $\Pi(0) = 0$. It receives contributions from the charged leptons (ℓ), the five light quarks u, d, s, c, b with the corresponding hadrons (h), and from the top quark:

$$
\Pi(q^2) = \Pi_\ell(q^2) + \Pi_h(q^2) + \Pi_{top}(q^2).
\tag{4.8}
$$

In particular, including a factor e^2 and considering the renormalized propagator, we obtain the running charge

$$
e^2 \to e^2(q^2) = \frac{e^2}{1 + \Pi(q^2)}.
\tag{4.9}
$$

In terms of the fine structure constant $\alpha = e^2/4\pi$ reads

$$
\alpha(q^2) = \frac{\alpha}{1 - \Delta\alpha(q^2)}.
\tag{4.10}
$$

As before, the various contributions to the shift in the fine structure constant come from the leptons (ℓ), the five light quarks (h) and from top quark:

$$
\Delta\alpha(q^2) = \Delta\alpha_\ell(q^2) + \Delta\alpha_h^{(5)}(q^2) + \Delta\alpha_{top}(q^2) + ...
\tag{4.11}
$$

While the other contributions can be calculated order by order in perturbation theory, the hadronic one exhibits low energy strong interaction effects and hence cannot be calculated by perturbative means.

A technique based on DRs is frequently used for the calculation of Feynman integrals, because the calculation of the imaginary part is simpler in general. They not only play a key role for the evaluation of non-perturbative hadronic effects but allow one to calculate numerically all kinds of vacuum polarization effects in higher order diagrams. Before we discuss this in more detail, let us summarize the key ingredients of the method:

- Optical theorem implied by unitarity: this states, in a scattering process framework, that the imaginary part of the forward scattering amplitude of an elastic process

$$
A + B \to A + B
\tag{4.12}
$$

is proportional to the sum over all possible final states $A + B \to$ "*anything*"

$$\mathrm{Im}\mathcal{M}_{forward}(A + B \to A + B) = \sqrt{\lambda(s, m^2, M^2)}\sigma_{tot}(A + B \to \text{``}anything\text{''}). \quad (4.13)$$

For the photon propagator it implies

$$\mathrm{Im}\Pi_\ell(s) = \frac{\alpha}{3}R(s), \quad (4.14)$$

where

$$R(s) = \sigma(e^+e^- \to \text{``}anything\text{''})/\frac{4\pi|\alpha(s)|^2}{3s}. \quad (4.15)$$

Taking into account the mass effects the $R(s)$ ratio which corresponds to the production of an electron-positron pair reads

$$R(s) = \sqrt{1 - \frac{4m^2}{s}}\left(1 + \frac{2m^2}{s}\right). \quad (4.16)$$

- Analyticity, implied by causality, may be expressed in form of a so-called subtracted dispersion relation

$$\frac{\Pi_\ell(q^2)}{q^2} = -\frac{1}{\pi}\int_{4m_\ell^2}^{\infty}\frac{dz}{z}\mathrm{Im}\Pi_\ell(z + i\epsilon)\frac{1}{q^2 - z + i\epsilon}, \quad (4.17)$$

where $\Pi_\ell(q^2)$ is the one-loop (renormalized) vacuum polarization function for a lepton ℓ in QED.

This result provides an alternative way to calculate the renormalized vacuum polarization function, namely, via DRs.

Within the context of calculating the leptonic NNLO QED contributions to μe scattering the most important application of DRs concerns the vacuum polarization contribution related to the non-factorizable diagrams of class IV.

Indeed, we calculated the amplitudes in class IV in the following way: the factor $\Pi_\ell(q^2)/q^2$ appearing in the loop—where q stands for the loop momentum—is replaced by the above dispersive integral (4.17), where q^2 appears only in the denominator of the term $1/(q^2 - z)$. Therefore, the dispersion relation effectively replaces the dressed propagator with a massive one, where z represents a fictitious squared photon mass. This allows us to interchange the integration order and evaluate, as a first step, the one-loop amplitudes with a massive photon. The results obtained for the z-dependent scattering amplitudes are then convoluted with the ratio $R(s)$.

We developed a *Mathematica* implementation using *FeynCalc* [54] and *Package-X* [70]. The results obtained for the z-dependent scattering amplitudes, in terms of scalar one-loop Passarino-Veltman integrals, were then convoluted with $\mathrm{Im}\Pi_\ell(s)$ and integrated numerically using analytic expressions given by *Package-X*. The use of *Mathematica*'s arbitrary-precision numbers allowed us to keep track of the precision at all steps and avoid instabilities during the numerical integration.

The lepton masses were kept different from zero throughout the calculation, so that the matrix elements were free of collinear singularities. Ultraviolet singularities were regularized via conventional dimensional regularization and UV-finite results were obtained in the on-shell remormalization scheme. The amplitudes of class II and the boxes of class IV develop IR poles which are cancelled by those arising from the phase space integration of the real emission diagrams of class III, as we will discuss in details in the next sections.

4.2   Results

4.2.1   Class 0

As we have seen before, the class 0 is characterized by QED tree-level diagram with a bubble of two-loop leptonic vacuum polarization inserted in the photon propagator. So the contribution of order $O(\alpha^4)$ from this diagram may be represented as follow:

$$\mathcal{X}_0^{NNLO} = \frac{1}{2}\text{Re}[(M_\gamma)^* \times M_{\Pi 2l}] = -2\Pi^{(4)}(q^2)\mathcal{X}_{LO} \tag{4.18}$$

In particular, the renormalized two-loop leptonic vacuum polarization takes the form:

$$\Pi^{(4)}(q^2) = \frac{\alpha^2}{16\pi^2}\Big(\frac{10}{3} + \frac{26}{3z} + \frac{2(1-16z)(1-z)G(z)^2}{3z} - \frac{4(1-z)(2z+3)G(z)}{z} - \\ - 2(2z+1)\Big(2(1-z)z\Big(\frac{F(z)}{z} - \frac{H(z)}{z^2}\Big) + \frac{H(z)}{z}\Big)\Big), \tag{4.19}$$

and

$$z = \frac{q^2}{4m_i^2} \qquad m_i = m, M, M_\tau, \tag{4.20}$$

$$y(z) = \frac{\sqrt{1-\frac{1}{z}} - 1}{\sqrt{1-\frac{1}{z}} + 1}, \tag{4.21}$$

$$G(z) = \frac{2y(z)\log(y(z))}{y(z)^2 - 1}, \tag{4.22}$$

$$F(z) = \frac{1}{(z-1)z}\Big[\log(-2z + 2\sqrt{z-1}\sqrt{z} + 1)\Big(-4\sqrt{z-1}\sqrt{z}\log\Big(\frac{2}{\sqrt{\frac{z-1}{z}} + 1}\Big) + \\ + (-3z + 3\sqrt{z-1}\sqrt{z} + 1)\log(-2z + 2\sqrt{z-1}\sqrt{z} + 1) - 8\sqrt{z-1}\sqrt{z}\times \\ \times \log(-2z + 2\sqrt{z-1}\sqrt{z} + 2)\Big) - 4\sqrt{z-1}\sqrt{z}(\mathcal{L}i_2(-z + 2\sqrt{z-1}\sqrt{z} + 1) + \\ + 2Li_2(2z - 2\sqrt{z-1}\sqrt{z} - 1))\Big], \tag{4.23}$$

$$H(z) = 6(4Li_3(-y(z)) + 2Li_3(y(z)) + \zeta(3)) - 8(2Li_2(-y(z)) + Li_2(y(z)))\log(y(z)) - \\ - 2(\log(1 - y(z)) + 2\log(1 + y(z)))\log^2(y(z)). \tag{4.24}$$

Therefore the NNLO scattering amplitude for class 0 results:

$$\mathcal{X}_0^{NNLO} = \frac{-128\pi^2\alpha^2 f(s,t)}{t^2}\Pi^{(4)}(t). \tag{4.25}$$

4.2.2 Class I

The class I is characterized by QED tree-level diagrams in combination with one or two one-loop leptonic vacuum polarization insertions. So the contributions of order $O(\alpha^4)$ from these diagrams may be addressed as follow:

$$\mathcal{X}_1^{NNLO} = \frac{1}{4}[\sum_{e,\mu,\tau}(M_\Pi)^2] + \frac{1}{2}\text{Re}[(M_\gamma)^* \times \sum_{e,\mu,\tau}M_{\Pi\Pi}], \tag{4.26}$$

where the sum runs over an electron, muon and tau bubble.

As in the previous case, we can consider the leptonic vacuum polarization insertion as a factorizable term and we exploit the results we have earlier obtained at NLO (already renormalized), using analytic expression given by *Package-X*,

$$\Pi_e(t) = \frac{\alpha\left(t(12m^2 + 5t) + 3\sqrt{t(t-4m^2)}(2m^2 + t)\log\left(\frac{\sqrt{t(t-4m^2)}+2m^2-t}{2m^2}\right)\right)}{9\pi t^2} \tag{4.27}$$

The contributions of the muon or tau vacuum polarization are obtained via the substitutions $m \to M$ and $m \to M_\tau$, respectively.

Eventually, inserting one or two times the Eq. (4.27) in the photon propagator of the LO scattering amplitude (3.15), we obtain

$$\begin{aligned}
\mathcal{X}_1^{NNLO} &= 3\mathcal{X}_{LO}(\sum_\ell \Pi_\ell(t))^2 \\
&= \frac{64\alpha^4 f(s,t)}{27t^6}\bigg(\sum_{m_i}\bigg(t(12m_i^2 + 5t) + 3\sqrt{t(t-4m_i^2)}(2m_i^2 + t)\times \\
&\quad \times \log\bigg(\frac{\sqrt{t(t-4m_i^2)}+2m_i^2-t}{2m_i^2}\bigg)\bigg)\bigg)^2
\end{aligned} \tag{4.28}$$

where $m_i = \{m, M, M_\tau\}$.

4.2.3 Class II

The class II is characterized by QED one-loop diagrams in combination with leptonic vacuum polarization insertion in the t-channel photon. In particular we have two different contributions to the differential cross-section

$$\begin{aligned}
\mathcal{X}_2^{NNLO} &= \mathcal{X}_{2,a}^{NNLO} + \mathcal{X}_{2,b}^{NNLO} \\
&= \frac{1}{2}\text{Re}[(M_\gamma)^* \times \sum_{i=e,\mu}M_{\Pi V_i}] + \frac{1}{2}\text{Re}[(M_\Pi)^* \times (\sum_{e,\mu}M_\Gamma + M_{bp} + M_{bc})],
\end{aligned} \tag{4.29}$$

where $M_{\Pi V_i}$ $(i = e, \mu)$ is the amplitude of the vertex correction diagrams with the insertion of a leptonic vacuum polarization in the photon propagator. The contributions of class II are proportional to $\Pi_\ell(t)$ and a combination of one-loop QED corrections at NLO of μe scattering.

As in the previous cases, we can consider the leptonic vacuum polarization insertion as a factorizable term (4.27) and we exploit the results we have already obtained at NLO concerning vertex and box corrections. As we have seen in Section 3.3, since the vertex diagram (3.33) is logarithmically UV divergent, we have to introduce a counterterm (3.34) to absorb the divergence and to obtain a finite result. On the other hand, making use of the Feynman rules and dimensional regularization, the box diagrams are not UV divergent. Consequently, we are left with the IR singularities, which we regularized through the introduction of a photon mass λ. We will discuss the IR divergences cancellation in details in Section 4.2.5, however we present here the structure of the IR part of the amplitude of class II:

$$\mathcal{X}_2^{IR} = -\Pi_\ell(t)[2\mathcal{X}_{1,Ve}^{IR} + 2\mathcal{X}_{1,V\mu}^{IR} + \mathcal{X}_{1,Bp}^{IR} + \mathcal{X}_{1,Bc}^{IR}], \tag{4.30}$$

where $\mathcal{X}_{1,i}^{IR}$ $(i = Ve, V\mu, Bp, Bc)$ represents the IR divergent part of the one-loop QED corrections.

Only after the summation with the soft NLO Bremsstrahlung contribution (class III) and the corrections of class IV, one is allowed to take the limit $\lambda \to 0$.

Therefore, the contribution of order $O(\alpha^4)$ to the differential cross section from class II yields

- The interference between the amplitude of the μe scattering at LO and the vertex correction diagrams with the insertion of a leptonic vacuum polarization in the photon propagator

$$\mathcal{X}_{2,\Pi V\mu}^{NNLO} = \frac{8\alpha^4}{9t^5(4M^2 - t)}\bigg[\sum_{m_i}\Big(t(12m^2 + 5t) + 3\sqrt{t(t - 4m^2)}(2m^2 + t)\times$$

$$\times \log\Big(\frac{\sqrt{t(t - 4m^2)} + 2m^2 - t}{2m^2}\Big)\Big]\times$$

$$\times \bigg[-4f(s,t)\Big(2t(8M^4 - 6M^2t + t^2)ScalarC0IR6(t, M, M)-$$

$$-\log M^2\Big(2t(t - 4M^2) + 2\sqrt{t(t - 4M^2)}(t - 2M^2)\times$$

$$\times \log\Big(\frac{\sqrt{t(t - 4M^2)} + 2M^2 - t}{2M^2}\Big)\Big) - 16M^2t-$$

$$- 8M^2\sqrt{t(t - 4M^2)}\log\Big(\frac{\sqrt{t(t - 4M^2)} + 2M^2 - t}{2M^2}\Big)+$$

$$+ 3t\sqrt{t(t - 4M^2)}\log\Big(\frac{\sqrt{t(t - 4M^2)} + 2M^2 - t}{2M^2}\Big) + 3t^2\Big)-$$

$$- 8M^2t(2m^2 + t)\Big(t - \sqrt{t(t - 4M^2)}\log\Big(\frac{\sqrt{t(t - 4M^2)} + 2M^2 - t}{2M^2}\Big)\Big)\bigg],$$
$$\tag{4.31}$$

where the sum runs over $m_i = \{m, M, M_\tau\}$ and it represents the contribution from the insertion of a leptonic vacuum polarization. And, $ScalarC0IR6(t, M, M)$ gives the finite part of Ellis-Zanderighi IR divergent triangle 6 [56], for t real and M positive.

In order to obtain the contribution from the diagram with the electron vertex correction $\mathcal{X}_{2,\Pi Ve}^{NNLO}$, we have just to perform the substitution $M \to m$. Therefore we obtain

$$\mathcal{X}_{2,a}^{NNLO} = \mathcal{X}_{2,\Pi V\mu}^{NNLO} + \mathcal{X}_{2,\Pi Ve}^{NNLO}. \tag{4.32}$$

- The interference between the amplitude of NLO leptonic vacuum polarization diagram and the vertex correction diagrams

$$\begin{aligned}
\mathcal{X}_{2,V\mu}^{NNLO} &= \frac{8\alpha^4}{9t^5(4M^2 - t)}\Bigg[\sum_{m_i}\Big(t(12m^2 + 5t) + 3\sqrt{t(t - 4m^2)}(2m^2 + t)\times \\
&\quad \times \log\Big(\frac{\sqrt{t(t - 4m^2)} + 2m^2 - t}{2m^2}\Big)\Big]\times \\
&\quad \times \Big[-4f(s,t)\Big(2t(8M^4 - 6M^2t + t^2)ScalarC0IR6(t, M, M) - \\
&\quad - \log M^2\Big(2t(t - 4M^2) + 2\sqrt{t(t - 4M^2)}(t - 2M^2)\times \\
&\quad \times \log\Big(\frac{\sqrt{t(t - 4M^2)} + 2M^2 - t}{2M^2}\Big)\Big) - 16M^2t - \\
&\quad - 8M^2\sqrt{t(t - 4M^2)}\log\Big(\frac{\sqrt{t(t - 4M^2)} + 2M^2 - t}{2M^2}\Big) + \\
&\quad + 3t\sqrt{t(t - 4M^2)}\log\Big(\frac{\sqrt{t(t - 4M^2)} + 2M^2 - t}{2M^2}\Big) + 3t^2\Big) - \\
&\quad - 8M^2t(2m^2 + t)\Big(t - \sqrt{t(t - 4M^2)}\log\Big(\frac{\sqrt{t(t - 4M^2)} + 2M^2 - t}{2M^2}\Big)\Big)\Bigg],
\end{aligned} \tag{4.33}$$

where the sum runs over $m_i = \{m, M, M_\tau\}$ and it represents the contribution from the insertion of a leptonic vacuum polarization. And, $ScalarC0IR6(t, M, M)$ gives the finite part of Ellis-Zanderighi IR divergent triangle 6 [56], for t real and M positive.

In order to obtain the contribution from the interference between the electron vertex correction and the NLO leptonic vacuum polarization diagram $\mathcal{X}_{2,Ve}^{NNLO}$, we have just to perform the substitution $M \to m$.

- At this point, we have to take into account the contribution that comes from the interference between the box diagrams and the NLO leptonic vacuum polarization

correction.

$$\mathcal{X}_{2,box}^{NNLO} = \frac{256\alpha^4\pi^4}{9t^3}\Bigg[\sum_{m_i}\Big(t(12m_i^2 + 5t) + 3\sqrt{t(t-4m_i^2)}(2m_i^2 + t)\times$$

$$\times \log\Big(\frac{\sqrt{t(t-4m_i^2)} + 2m_i^2 - t}{2m_i^2}\Big)\Big)\Bigg]\Big[b_0 + b_1 B_0(0, m^2, m^2)+$$
$$+ b_2 B_0(0, M^2, M^2) + b_3 B_0(s, m^2, M^2) + b_4 B_0(2M^2 + 2m^2 - s - t, m^2, M^2)+$$
$$+ b_5 B_0(t, 0, 0) + b_6 C_0(m^2, m^2, t, 0, m^2, 0)+$$
$$+ b_7 C_0(M^2, M^2, t, 0, M^2, 0) + b_8 C_0(m^2, M^2, s, m^2, \lambda^2, M^2)+$$
$$+ b_9 C_0(m^2, M^2, 2m^2 + 2M^2 - s - t, m^2, \lambda^2, M^2)+$$
$$+ b_{10}D_0(m^2, m^2, M^2, M^2, t, s, \lambda^2, m^2, \lambda^2, M^2)+$$
$$+ b_{11}D_0(m^2, m^2, M^2, M^2, t, 2M^2 + 2m^2 - s - t, m^2, \lambda^2, M^2)\Big]$$

$$(4.34)$$

where the sum runs over $m_i = \{m, M, M_\tau\}$ and it represents the contribution from the insertion of a leptonic vacuum polarization. And, we have

$$b_0 = \frac{-32m^2(m^2 - M^2 + s)}{t - 4M^2} + \frac{-32M^2(-m^2 + M^2 + s)}{t - 4M^2} - 8(m^2 + M^2)-$$
$$- \frac{8t((m^2 - M^2)^2 - s(m^2 + M^2))}{m^4 - 2m^2(M^2 + s) + (M^2 - s)^2} - \frac{4(m - M)^2((m + M)^2 - s)}{(m + M)^2 - s - t}+ \qquad (4.35)$$
$$+ \frac{4(m + M)^2((m - M)^2 - s)}{-(m + M)^2 + s + t},$$

$$b_1 = 2m\Big(-\frac{8m(m^2 - M^2 + s)}{t - 4m^2} + \frac{2mt(-m^2 + M^2 + s)}{m^4 - 2m^2(M^2 + s) + (M^2 - s)^2}+$$
$$+ \frac{(m + M)(s - (m - M)^2)}{(m - M)^2 - s - t} + \frac{(m - M)(s - (m + M)^2)}{(m + M)^2 - s - t} - 2m\Big), \qquad (4.36)$$

$$b_2 = 2M\Big(-\frac{8M(-m^2 + M^2 + s)}{t - 4M^2} + \frac{2Mt(m^2 - M^2 + s)}{m^4 - 2m^2(M^2 + s) + (M^2 - s)^2}+$$
$$+ \frac{(m + M)(s - (m - M)^2)}{(m - M)^2 - s - t} + \frac{(m - M)(-s + (m + M)^2)}{(m + M)^2 - s - t} - 2M\Big), \qquad (4.37)$$

$$b_3 = \frac{2(m^6 + (M^2 - s)^3 + (M^4 - s^2)t + m^4(-M^2 - 3s + t))}{m^4 - 2m^2(M^2 + s) + (M^2 - s)^2}+$$
$$+ \frac{2(-m^2(M^4 - 3s^2 + 2M^2(s + t)))}{m^4 - 2m^2(M^2 + s) + (M^2 - s)^2}, \qquad (4.38)$$

$$b_4 = \frac{2(m^6 + (M^2 - s)^3 - m^4(M^2 + 3s) - t^2(M^2 + s))}{((m - M)^2 - s - t)((m + M)^2 - s - t)}+$$
$$+ \frac{2(-m^2(M^4 + 2M^2(s - 4t) - (3s - t)(s + t)) + 2st(M^2 - s))}{((m - M)^2 - s - t)((m + M)^2 - s - t)}, \qquad (4.39)$$

$$b_5 = -\frac{2(4mM - t)(4mM + t)(2(m^2 + M^2 - s) - t)}{(4m^2 - t)(-4M^2 + t)}, \tag{4.40}$$

$$b_6 = -\frac{2(8m^4 - 8m^2t + t^2)(2(m^2 + M^2 - s) - t)}{(4m^2 - t)}, \tag{4.41}$$

$$b_7 = -\frac{2(8M^4 - 8M^2t + t^2)(2(m^2 + M^2 - s) - t)}{(4M^2 - t)}, \tag{4.42}$$

$$b_8 = 2(m^2 + M^2 - s)(2s + t), \tag{4.43}$$

$$b_9 = 2(4m^2 + 4M^2 - 2s - t)(m^2 + M^2 - s - t), \tag{4.44}$$

$$b_{10} = (m^2 + M^2 - s)(4(m^2 + M^2 - s)^2 + 2st + t^2), \tag{4.45}$$

$$b_{11} = (m^2 + M^2 - s - t)(4(m^2 + M^2 - s)^2 - 4(m^2 + M^2)t + 6st + 3t^2). \tag{4.46}$$

Therefore we obtain

$$\mathcal{X}_{2,b} = \mathcal{X}_{2,V\mu} + \mathcal{X}_{2,Ve} + \mathcal{X}_{2,box}. \tag{4.47}$$

Finally, we have all the ingredients to evaluate the contribution given by the class II, as we have seen in (4.29).

4.2.4 Class III

The class III contribution is made of real-emission diagrams with a leptonic vacuum polarization insertion in the *t*-channel photon.

Up to this point, we have regularized only the UV singularities. And, as we have seen for the NLO contributions, keeping a finite m complicated the computation of the virtual correction, but it is necessary to regularize the collinear divergences. We are left with only soft singularities, regularized through the introduction of a fictitious photon mass λ.

The contribution of order $O(\alpha^4)$ to the differential cross section from the real emission is given by

$$\mathcal{X}_3^{NNLO} = \frac{1}{2}\text{Re}[(M_{Br}^{LO})^* \times M_{Br}^{NLO}], \tag{4.48}$$

which is proportional to $\Pi_\ell(t)$. Since the vacuum polarization term can be factorized, we exploit the results already obtained at NLO. In particular, we consider soft photon emission both in the initial and in the final state, in this soft limit the emitted photon has an energy lower than an experimental small threshold ω.

Also in this case, the squared amplitude for our process is easy to evaluate with an additional phase-space integration for the photon variable k (3.58).

We followed the approach proposed by 't Hooft and Veltman in [55] and reported in details in Appendix B.

In light of this, we expect that the IR part of the amplitude of class III is

$$\mathcal{X}_3^{IR} = -\Pi_\ell(t)[2\mathcal{X}_{0,Br}^{IR}], \tag{4.49}$$

where $\mathcal{X}_{0,Br}^{IR}$ represents the soft LO Bremsstrahlung QED contribution. Insofar, we obtain

$$
\begin{aligned}
\mathcal{X}_3^{NNLO} = \frac{256\pi^2\alpha^4}{9t^4} 2f(s,t) \Big[& \sum_{m_i} \Big(t(12m_i^2 + 5t) + 3\sqrt{t(t-4m_i^2)}(2m_i^2 + t) \times \\
& \times \log\Big(\frac{\sqrt{t(t-4m_i^2)} + 2m_i^2 - t}{2m_i^2} \Big) \Big) \Big] \Big[-(2M^2 - t)\mathcal{I}(p_1, p_3) - \\
& - (2m^2 - t)\mathcal{I}(p_2, p_4) - 2(m^2 + M^2 - s)\mathcal{I}(p_1, p_2) + 2M^2\mathcal{I}(p_1, p_1) + \\
& + 2m^2\mathcal{I}(p_2, p_2) - 2(m^2 + M^2 - u)\mathcal{I}(p_2, p_3) \Big],
\end{aligned}
\tag{4.50}
$$

where the sum runs over $m_i = \{m, M, M_\tau\}$ and it represents the contribution from the insertion of a leptonic vacuum polarization. In this section we keep the implicit form of the integrals $\mathcal{I}(p_i, p_j)$, while their evaluation is quoted in Appendix B.

Taking the sum between two-loop virtual contributions and the soft Bremsstrahlung diagrams of class III we obtain the cancellation of IR divergences. In particular, we will discuss later how to treat the IR singularities in the context of non-factorizable diagrams of class IV.

Only at this point, we can safely take the limit $\lambda \to 0$. In particular, we remember that $C_0(m^2, m^2, t, 0, m^2, 0)$ and $C_0(M^2, M^2, t, 0, M^2, 0)$, showing up in the box contributions, are already IR finite, differently from all the other three- and four-point Passarino-Veltman functions [56].

As we have already underlined, the MUonE experiment is not expected to detect photons in the final state. Therefore, the theoretical needed result to match MUonE's measurements should include also the hard Bremsstrahlung contributions to obtain a physical result.

4.2.5   Class IV

As previously anticipated, the evaluation of the leptonic NNLO QED corrections is complicated by the presence of non-factorizable two-loop diagrams. Indeed, the class IV is characterized by one-loop QED amplitudes with a leptonic vacuum polarization insertion in the loop. They can be further subdivided into vertex and box corrections.

We will present their calculation using the dispersive approach, based on the subtracted dispersion relation (4.17). The dispersion relation replaces the free photon propagator in the one-loop graph with a massive one, where z represents the fictitious squared photon mass,

$$
\frac{-ig^{\mu\nu}}{q^2} \to \frac{-ig^{\mu\nu}}{q^2 - z}.
\tag{4.51}
$$

The result afterward has to be convoluted with the imaginary part of the photon vacuum polarization. In particular, the factor $\Pi_\ell(q^2)/q^2$ appearing in the loop—where q^2 is the loop momentum—is replaced by the right hand side of Eq. (4.17).

Now, let's focus on the vertex diagram, the contribution of order $O(\alpha^4)$ comes from:

$$
\mathcal{X}_{4,ver}^{NNLO} = \frac{1}{2}\text{Re}[(M_\gamma)^* \times \sum_{e,\mu}(M_{\Gamma\Pi})].
\tag{4.52}
$$

We known that we can rewrite our vertex through the form factors, as in the Eq. (2.14). Hence, we obtain:

$$
\begin{aligned}
F_{1,M}(t,z) = \frac{\alpha}{4\pi M^2(t-4M^2)^2}\Big(& 2t(-4M^4 + M^2(t+7z) - tz)B_0(M^2, M^2, z) - \\
& - M^2(32M^4 - 4M^2(5t - 4z) + t(3t + 2z))B_0(t, M^2, M^2) + \\
& + (4M^2 - t)(8M^4 - M^2(t - 4z) - tz)B_0(0, M^2, M^2) + \\
& + t(4M^2 - t)(M^2 - z) + tz(t - 4M^2)B_0(0, z, z) - \\
& - (t - 4M^2)^2(4M^2 - z)C_0(M^2, M^2, 0, M^2, z, M^2) + \\
& + 2M^2(32M^6 - 32M^4 t + 2M^2(5t^2 + 4tz - 4z^2) - \\
& - t(t + z)^2)C_0(M^2, M^2, t, M^2, z, M^2)\Big),
\end{aligned}
$$

(4.53)

$$
\begin{aligned}
F_{2,M}(t,z) = \frac{-i\alpha}{2\pi M(t-4M^2)^2}\Big(& (-8M^4 + 2M^2(t+5z) - tz)B_0(M^2, M^2, z) + \\
& + M^2(4M^2 - t - 6z)B_0(t, M^2, M^2) + z(t - 4M^2)B_0(0, z, z) + \\
& + M^2(4M^2 - t)B_0(0, M^2, M^2) + (4M^2 - t)(M^2 - z) + \\
& + 2M^2 z(8M^2 - 2t - 3z)C_0(M^2, M^2, t, M^2, z, M^2)\Big).
\end{aligned}
$$

(4.54)

The results obtained for the z-dependent scattering amplitudes, in terms of scalar one-loop Passarino-Veltman integrals, were then convoluted with $\mathrm{Im}\Pi_\ell(s)$ and integrated numerically, using analytic expressions given by *Package-X*. The use of *Mathematica*'s arbitrary-precision numbers allowed us to keep track of the precision at all steps and avoid instabilities during the numerical integration. In order to obtain the form factors for the electron vertex and perform the numerical integration for this correction we have to consider the substitution $M \to m$. In particular, we underline that this result is IR finite. This is related to the fact that we have introduced a fictitious squared mass for the photon that is inserted into an integral, and we don't have any other photon in the loop that can bring an IR divergence.

At this point, let's focus on the box diagrams. In particular we have four contributions, depending on which photon contains the leptonic vacuum polarization (considering also the crossed diagrams). However it's easy to see that the two contributions, coming from the insertion of a vacuum polarization in the right or left photon in the planar box diagrams, are equal; and so also the crossed box contributions. Therefore we can safely take

$$
\mathcal{X}_{4,box}^{NNLO} = \frac{1}{2}\mathrm{Re}[(M_\gamma)^* \times 2M_{bp\Pi}] + \frac{1}{2}\mathrm{Re}[(M_\gamma)^* \times 2M_{bc\Pi}].
$$

(4.55)

Insofar, we obtain

$$
\begin{aligned}
\mathcal{X}_{4,box}^{NNLO} = \frac{32\alpha^3\pi}{t}\Big[& d_0 + d_1(B_0(0,m^2,m^2) + B_0(m^2,m^2,z)) + \\
& + d_2(B_0(0,M^2,M^2) + B_0(M^2,M^2,z)) + d_3 B_0(s,m^2,M^2) + \\
& + d_4 B_0(2m^2 + 2M^2 - s - t, m^2, M^2) + d_5 B_0(t,0,z) + \\
& + d_6 C_0(m^2,m^2,t,0,m^2,z) + d_7 C_0(m^2,M^2,s,m^2,0,M^2) + \\
& + d_8 C_0(m^2,M^2,s,m^2,z,M^2) + d_9 C_0(m^2,M^2,u,m^2,0,M^2) + \\
& + d_{10} C_0(m^2,M^2,u,m^2,z,M^2) + d_{11} C_0(M^2,M^2,t,0,M^2,z) + \\
& + d_{12} D_0(m^2,m^2,M^2,M^2,t,s,0,m^2,z,M^2) + \\
& + d_{13} D_0(m^2,m^2,M^2,M^2,t,u,0,m^2,z,M^2)\Big],
\end{aligned}
\tag{4.56}
$$

where,

$$
\begin{aligned}
d_0 = 2\Big(& 2(m^2 + M^2) + \frac{(m+M)^2((m-M)^2 - s)}{(m-M)^2 - s - t} + \frac{(m-M)^2((m+M)^2 - s)}{(m+M)^2 - s - t} + \\
& + \frac{2t((m^2 - M^2)^2 - s(m^2 + M^2))}{m^4 - 2m^2(M^2 + s) + (M^2 - s)^2} + \frac{8m^2(m^2 - M^2 + s)}{-4m^2 + t} + \frac{8M^2(-m^2 + M^2 + s)}{-4M^2 + t}\Big),
\end{aligned}
\tag{4.57}
$$

$$
\begin{aligned}
d_1 = m\Big(& \frac{8m(m^2 - M^2 + s)}{t - 4m^2} + \frac{2mt(m^2 - M^2 - s)}{m^4 - 2m^2(M^2 + s) + (M^2 - s)^2} + \\
& + \frac{(m+M)((m-M)^2 - s)}{(m-M)^2 - s - t} + \frac{(m-M)((m+M)^2 - s)}{(m+M)^2 - s - t} + 2m\Big),
\end{aligned}
\tag{4.58}
$$

$$
\begin{aligned}
d_2 = M\Big(& \frac{8M(-m^2 + M^2 + s)}{t - 4M^2} + \frac{2Mt(-m^2 + M^2 - s)}{m^4 - 2m^2(M^2 + s) + (M^2 - s)^2} + \\
& + \frac{(m+M)((m-M)^2 - s)}{(m-M)^2 - s - t} + \frac{(m-M)(-(m+M)^2 + s)}{(m+M)^2 - s - t} + 2M\Big),
\end{aligned}
\tag{4.59}
$$

$$
\begin{aligned}
d_3 = & -\frac{2(m^6 + (M^2 - s)^3 + (M^4 - s^2)t + m^4(-M^2 - 3s + t))}{m^4 - 2m^2(M^2 + s) + (M^2 - s)^2} - \\
& - \frac{2(-m^2(M^4 - 3s^2 + 2M^2(s + t)))}{m^4 - 2m^2(M^2 + s) + (M^2 - s)^2},
\end{aligned}
\tag{4.60}
$$

$$
\begin{aligned}
d_4 = & \frac{2(-m^6 - (M^2 - s)^3 + m^4(M^2 + 3s) + t^2(M^2 + s))}{((m-M)^2 - s - t)((m+M)^2 - s - t)} + \\
& + \frac{2(m^2(M^4 + 2M^2(s - 4t) - (3s - t)(s + t)) + 2st(-M^2 + s))}{((m-M)^2 - s - t)((m+M)^2 - s - t)},
\end{aligned}
\tag{4.61}
$$

$$
d_5 = \frac{2(4mM - t)(4mM + t)(2(m^2 + M^2 - s) - t)}{(4m^2 - t)(-4M^2 + t)},
\tag{4.62}
$$

$$
d_6 = \frac{2(8m^4 + t^2 + 2m^2(-4t + z))(2(m^2 + M^2 - s) - t)}{(4m^2 - t)},
\tag{4.63}
$$

$$d_7 = -(m^2 + M^2 - s)(2s + t + z), \tag{4.64}$$

$$d_8 = \frac{-((m - M)^2 - s)(m^2 + M^2 - s)((m + M)^2 - s)(2s + t)}{m^4 - 2m^2(M^2 + s) + (M^2 - s)} +$$
$$+ \frac{(-m^6 - (M^2 - s)^3 + m^4(M^2 + 3s - 2t) + 2M^2(-M^2 + s)t)z}{m^4 - 2m^2(M^2 + s) + (M^2 - s)} +$$
$$+ \frac{(m^2(M^4 + s(-3s + 2t) + 2M^2(s + 2t)))z}{m^4 - 2m^2(M^2 + s) + (M^2 - s)}, \tag{4.65}$$

$$d_9 = -(4m^2 + 4M^2 - 2s - t + z)(m^2 + M^2 - s - t), \tag{4.66}$$

$$d_{10} = \frac{-4m^8 - (4M^2 - 2s - t)(M^2 - s - t)^3 + m^6(14s + 13t - z)}{((m - M)^2 - s - t)((m + M)^2 - s - t)} +$$
$$+ \frac{-(M^2 - s - t)(M^4 - 2M^2s + (s + t)^2)z}{((m - M)^2 - s - t)((m + M)^2 - s - t)} +$$
$$+ \frac{m^4(8M^4 - 3(s + t)(6s + 5t)(3s + t)z + M^2(18s + 19t + z))}{((m - M)^2 - s - t)((m + M)^2 - s - t)} +$$
$$+ \frac{m^2(M^4(18s + 19t + z) - 2M^2(14s^2 + 27st + 13t^2 - sz + 5tz))}{((m - M)^2 - s - t)((m + M)^2 - s - t)} +$$
$$+ \frac{m^2((s + t)((s + t)(10s + 7t) - (3s + t)z))}{((m - M)^2 - s - t)((m + M)^2 - s - t)}, \tag{4.67}$$

$$d_{11} = \frac{2(2(m^2 + M^2 - s) - t)(8M^4 + t^2 + 2M^2(-4t + z))}{4M^2 - t}, \tag{4.68}$$

$$d_{12} = -(m^2 + M^2 - s)(4m^4 + 4M^4 + 8m^2(M^2 - s) - 8M^2s + 4s^2 +$$
$$+ 2st + t^2 + 2sz + z^2) \tag{4.69}$$

$$d_{13} = -(m^2 + M^2 - s - t)(4m^4 + 4M^4 + 4s^2 + 6st + 3t^2 - 4M^2(2s + t + z) -$$
$$- 2(s + t)z + z^2 + 4m^2(2M^2 - 2s - t + z)). \tag{4.70}$$

The results obtained for the z-dependent scattering amplitudes, in terms of scalar one-loop Passarino-Veltman integrals, were then convoluted with $\text{Im}\Pi_\ell(s)$ and integrated numerically, using analytic expressions given by *Package-X*. Once again, the use of *Mathematica*'s arbitrary-precision numbers allowed us to keep track of the precision at all steps and avoid instabilities during the numerical integration.

Notice that the box diagrams are IR divergent, however we don't introduce a fictitious photon mass λ, as we performed at NLO, in order to obtain a finite results. This is related to the fact that *Package-X* uses dimensional regularization also for the IR singularities, nevertheless there is a one-to-one correspondence between the $1/\tilde{\epsilon}$ pole[1] of *Package-X* and the term $\log \lambda$, indeed

$$2 \log \lambda \leftrightarrow \frac{1}{\epsilon} - \gamma + \log 4\pi + \log \mu^2. \tag{4.71}$$

We have seen at NLO that the cancellation of the IR divergences is given by

$$\mathcal{X}_{0,Br}^{IR} + \mathcal{X}_{1,V\mu}^{IR} + \mathcal{X}_{1,Ve}^{IR} + \mathcal{X}_{1,Bp}^{IR} + \mathcal{X}_{1,Bc}^{IR} = 0 \tag{4.72}$$

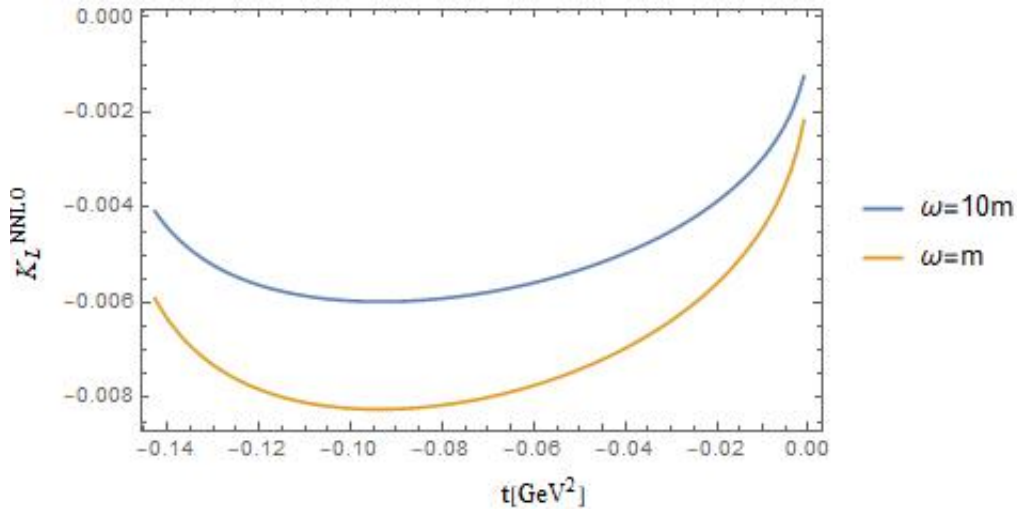[1]This corresponds to $\frac{1}{\epsilon} - \gamma + \log 4\pi$.

Figure 4.2: $K_\ell^{NNLO}(t)$ factor for a negative muon beam of energy $E_\mu = 150$ GeV, characterized by different threshold energy for the real emission of class III. This result should not be employed in the limit $t \to t_{min}$.

where $\mathcal{X}_{0,Br}^{IR}$ represents the soft LO Bremsstrahlung QED contribution and $\mathcal{X}_{1,i}^{IR}$ ($i = Ve, V\mu, Bp, Bc$) is the IR divergent part of the one-loop QED corrections.

Since the equations (4.30) and (4.49) are valid, and we want to obtain a differential cross section which is IR finite, exploiting the previous result (4.72), we need to find out the structure of the terms related to the IR poles of box diagrams of class IV. The evaluation of these terms seems to be complicated by the fact that they are included in an integration over z. However, if we focus only on the $1/\tilde\epsilon$ terms, we obtain

$$\mathcal{X}_{4,box}^{IR} = \int_{4m^2}^\infty dz \frac{\mathrm{Im}\Pi_\ell(z) f^{IR}(s,t,u)}{\pi z(t-z)}, \tag{4.73}$$

where $f^{IR}(s,t,u)$ is a generic function of our Mandelstam variables s,t and u. Surprisingly, this represents our dispersive integral (4.17), therefore we can write

$$\mathcal{X}_{4,box}^{IR} = -\Pi_\ell(t) \frac{f^{IR}(s,t,u)}{t} \tag{4.74}$$

Summing up (4.30), (4.49) and this last result, we obtain the cancellation of the IR divergences.

4.2.6   NNLO QED leptonic corrections

The ratio of the NNLO QED leptonic corrections to the μe differential cross section, with respect to the squared momentum transfer t, and the LO prediction,

$$K_\ell^{NNLO}(t) = \frac{d\sigma_\ell^{NNLO}}{dt} \Big/ \frac{d\sigma_0}{dt}, \tag{4.75}$$

is shown in Fig. 4.2 for the process $\mu^- e^- \to \mu^- e^-$ for $E_\mu = 150$ GeV.[2]

It is important to underline that, for the evaluation of the ratio K_ℓ^{NNLO}, we considered only the soft Bemsstrahlung emission in class III. This means that our result strongly depends on the value of threshold ω we chose. As MUonE does not detect photons, in order to obtain a result comparable to its experimental data, we need to add to our evaluation the hard Bremsstrahlung contributions.

In the light of what we said before, Figure 4.2 shows that, when the muon beam has an energy of 150 GeV, the factor $K_\ell^{NNLO}(t)$ is of order $10^{-3} - 10^{-4}$, for the most of the kinematic region scanned by the squared momentum transfer t and for photon energy cuts of order $(1 - 10)$ MeV. These corrections are therefore larger than the $O(10^{-5})$ precision expected at the MUonE experiment.

The above numerical method is analogous to that employed for the recent determination of the NNLO hadronic corrections addressed in Ref. [68]. However, we expect that the evaluation of NNLO ratio $K_\ell(t)$ shows higher values than the corrections obtained for the hadronic vacuum polarization, because of the large leptonic contributions to the vacuum polarization.

---

[2]Our result is specific to $\mu^- e^- \to \mu^- e^-$. For $\mu^+ e^- \to \mu^+ e^-$ the box diagrams in classes II and IV are equal in size but with opposite sign for μ^+ and μ^-. The same pattern is observed at NLO [53].

Chapter 5

Conclusions

In this thesis we calculated the NLO and NNLO QED leptonic corrections to the differential cross section for the process $\mu^- e^- \to \mu^- e^- (+\gamma)$, where $(+\gamma)$ indicates the possible emission of photon, relevant to the recently proposed MUonE experiment at CERN. The MUonE experiment proposes to determine the leading hadronic contribution to a_μ, measuring the shape of the differential cross section of muon-electron elastic scattering in the space-like region. In order for this new determination of the leading hadronic corrections to be competitive, the shape of the μe differential cross-section must be measured with a systematic uncertainty of $O(10^{-5})$ close to the kinematic endpoint.

We showed that, in a fixed target experiment where the electron is initially at rest and the energy of the incoming muons (or antimuons) is 150 GeV, the QED leptonic corrections at NNLO to the differential cross-section with respect to t are of order $10^{-3} - 10^{-4}$, for the most of the kinematic region spanned by t and for photon energy cuts of order $(1-10)$ MeV. Therefore, these corrections will play a crucial role in the data analysis of future high-precision muon-electron scattering experiment like MUonE, whose goal is to reach a relative precision of order 10 ppm.

The NLO QED corrections are already present in the literature and, recently, a fully differential NLO code has been used to perform a detailed phenomenological study, taking into account the full m dependence [53]. We analyzed the NLO QED corrections, verifying the correspondence with the results in literature. Moreover, these contributions represent the benchmark for the evaluation of leptonic QED NNLO corrections.

On the other hand, a complete analytical result for NNLO QED corrections to μe scattering is not yet available. However we have exploited the subtracted dispersion relation to calculate numerically the leptonic NNLO QED corrections, i.e. the class of leptonic NNLO QED contributions arising from two-loop QED diagrams with leptonic vacuum polarization insertions in the photon propagator, taking the full electron and muon mass dependence. Indeed, dispersion relations allow one to calculate numerically all kinds of vacuum polarization effects in higher order diagrams.

The numerical method employed in this thesis is analogous to that presented in the recent determination of the NNLO hadronic corrections addressed in Ref. [68]. However, with respect to the hadronic case, we now have the advantage that we know the analytic

expression of the leptonic vacuum polarization function $\text{Im}\Pi_\ell(s)$. Therefore, this could represents an important tool in order to compute analytically the NNLO leptonic corrections. These analytic expressions would give us the opportunity, not only to check our numerical results, but also to extract the electron mass dependence of these NNLO corrections. In fact, for example, the master integrals for the two-loop planar and non-planar four-point Feynman diagrams were calculated in Refs. [62, 63] setting the electron mass to zero (while retaining full dependence on the muon one). In particular, having the analytic results of the NNLO leptonic corrections, would allow us to explore the extraction of the leading electron mass effects (leading logarithmic terms $\log(m)$) from the massless two-loop μe scattering amplitudes, which has been addressed in [44, 65].

We have discussed the computation of the μe differential cross section in a strict expansion in the coupling α. At N^{n}LO the cross section contains large logarithms of the form

$$\alpha^2 \times (\alpha L_m)^n = \alpha^2 \times \alpha^n \log^n \frac{m^2}{Q^2} \tag{5.1}$$

that potentially invalidate the perturbative expansion, since αL_m is not necessary a good expansion parameter. In fact, the full NNLO QED corrections to the μe differential cross section, with respect to the squared momentum transfer t, contain a term which diverges logarithmically at the end of the electron spectrum. This feature, clearly visible in the results of Ref. [68], is related to the infrared divergence, indicating a breakdown of the perturbative expansion and the need for resummation. This will be the topic of further investigations.

Appendix A

Conventions and useful formulas

A.1   Feynman rules

- **External lines**

$$u(\vec{p}) = \quad \xrightarrow{\quad p \quad} \bullet \qquad\qquad \bar{u}(\vec{p}) = \bullet \xrightarrow{\quad p \quad} \qquad\qquad \text{(A.1)}$$

$$\epsilon_r^\mu(\vec{k}) = \quad \wwwww\hspace{-1pt}\xrightarrow{\quad k \quad}\bullet \qquad\qquad \epsilon_r^{\mu*}(\vec{k}) = \bullet\wwwww\xrightarrow{\quad k \quad} \qquad\qquad \text{(A.2)}$$

- **Propagators**

  We assume the unitary gauge, and the prescription $i\epsilon$ is omitted.

$$Photon: \quad \mu \;\wwwww\xrightarrow{\quad k \quad}\; \nu \quad = \frac{-ig^{\mu\nu}}{k^2}$$
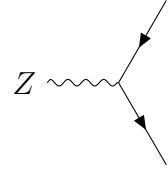
$$Fermion: \quad \xrightarrow{\quad p \quad} \quad = \frac{i(\not{p}+m)}{p^2-m^2} \qquad\qquad \text{(A.3)}$$

$$Massive\ Vector\ Boson: \quad \mu \;\wwwww\xrightarrow{\quad k \quad}\; \nu \quad = \frac{i(-g^{\mu\nu}+\frac{k^\mu k^\nu}{M_z^2})}{k^2-M_Z^2}$$

- **Vertices**

$$\gamma\;\wwwww\!\!\!\diagup = -ie\gamma^\mu \qquad\qquad \text{(A.4)}$$

$$Z \sim\!\!\!\sim\!\!\!\sim\!\!\!< \quad = \frac{-ig\gamma^\mu}{2\cos\theta_\omega}(g_V - g_A\gamma^5) \tag{A.5}$$

A.2 Dirac Algebra

$$\{\gamma^\mu, \gamma^\nu\} = 2g^{\mu\nu} \tag{A.6}$$

$$\gamma^5 = i\gamma^0\gamma^1\gamma^2\gamma^3 \tag{A.7}$$

with

$$\{\gamma^\mu, \gamma^5\} = 0 \qquad (\gamma^5)^2 = \mathbf{1} \qquad (\gamma^5)^\dagger = \gamma^5 \tag{A.8}$$

and

$$\sigma^{\mu\nu} = \frac{i}{2}[\gamma^\mu, \gamma^\nu] \tag{A.9}$$

- **Traces**

$$
\begin{aligned}
\mathrm{Tr}[\gamma^\mu, \gamma^\nu] &= 4g^{\mu\nu}, \\
\mathrm{Tr}[\gamma^\mu, \gamma^\nu, \gamma^\rho, \gamma^\sigma] &= 4(g^{\mu\nu}g^{\rho\sigma} - g^{\mu\rho}g^{\nu\sigma} + g^{\mu\sigma}g^{\nu\rho}), \\
\mathrm{Tr}[odd~number~of~\gamma's] &= 0, \\
\mathrm{Tr}[\gamma^5] &= 0, \\
\mathrm{Tr}[\gamma^\mu, \gamma^5] &= 0, \\
\mathrm{Tr}[\gamma^\mu, \gamma^\nu, \gamma^5] &= 0, \\
\mathrm{Tr}[\gamma^\mu, \gamma^\nu, \gamma^\rho, \gamma^5] &= 0, \\
\mathrm{Tr}[\gamma^\mu, \gamma^\nu, \gamma^\rho, \gamma^\sigma, \gamma^5] &= -4i\epsilon^{\mu\nu\rho\sigma}.
\end{aligned}
\tag{A.10}
$$

- **Contraction Identities in D-dimensions**

$$
\begin{aligned}
g^{\mu\nu}g_{\mu\nu} &= D, \\
\gamma^\mu\gamma_\mu &= D, \\
\gamma^\mu\gamma^\nu\gamma_\mu &= (2-D)\gamma^\nu, \\
\gamma^\mu\gamma^\nu\gamma^\rho\gamma_\mu &= 4g^{\nu\rho} + (D-4)\gamma^\nu\gamma^\rho, \\
\gamma^\mu\gamma^\nu\gamma^\rho\gamma^\sigma\gamma_\mu &= -2\gamma^\sigma\gamma^\rho\gamma^\nu + (4-D)\gamma^\nu\gamma^\rho\gamma^\sigma.
\end{aligned}
\tag{A.11}
$$

- **Dirac Equation in Momentum Space**

$$(\not{p} - m)u(p) = 0 \qquad\qquad \bar{u}(p)(\not{p} - m) = 0 \tag{A.12}$$

$$(\not{p} + m)v(p) = 0 \qquad\qquad \bar{v}(p)(\not{p} + m) = 0 \tag{A.13}$$

Appendix B

Scalar Integrals

B.1 Passarino Veltman Decomposition

In this appendix we give a brief introduction to the technique of PV decomposition [71] for one-loop integrals.

Assuming dimensional regularization $d = 4 - \epsilon$, a generic one-loop tensor integral is defined as

$$T_n^{\mu_1,...,\mu_\rho} = \frac{(2\pi\mu)^{4-d}}{i\pi^2} \int d^d k \frac{k^{\mu_1}....k^{\mu_\rho}}{D_0 D_1 D_2 ... D_{n-1}} \tag{B.1}$$

where a denominator D_i is given by [1]

$$D_i = (k + r_i)^2 - m_i^2. \tag{B.2}$$

Since p_i are the external momenta entering in the loop, then

$$\begin{aligned} r_j &= \sum_{i=1}^{j} p_i \qquad (j = 1, ..., n-1) \\ r_0 &= \sum_{i=1}^{n} p_i = 0. \end{aligned} \tag{B.3}$$

Exploiting the Lorentz covariance of tensor integrals, these can be written as a linear combination of the external momenta and the metric tensor $g^{\mu\nu}$ using a set of coefficient functions. Moreover, it is shown that all the tensor integrals can be decomposed in terms of only four independent scalar integrals with one, two, three or four denominators,

---

[1] The prescription $i\epsilon$ is omitted

denoted as:

$$A_0(m_0^2) = \frac{(2\pi\mu)\epsilon}{i\pi^2} \int d^d k \frac{1}{k^2 - m_0^2}$$

$$B_0(r_{10}^2, m_0^2, m_1^2) = \frac{(2\pi\mu)^\epsilon}{i\pi^2} \int d^d k \prod_{i=0}^{1} \frac{1}{[(k + r_i)^2 - m_i^2]}$$

$$C_0(r_{10}^2, r_{12}^2, r_{20}^2, m_0^2, m_1^2, m_2^2) = \frac{(2\pi\mu)^\epsilon}{i\pi^2} \int d^d k \prod_{i=0}^{2} \frac{1}{[(k + r_i)^2 - m_i^2]} \tag{B.4}$$

$$D_0(r_{10}^2, r_{12}^2, r_{23}^2, r_{30}^2, r_{20}^2, r_{13}^2, m_0^2, m_1^2, m_2^2, m_3^2) = \frac{(2\pi\mu)^\epsilon}{i\pi^2} \int d^d k \prod_{i=0}^{3} \frac{1}{[(k + r_i)^2 - m_i^2]}$$

where

$$r_{ij}^2 = (r_i - r_j)^2 \qquad \forall i, j = (0, n - 1). \tag{B.5}$$

These scalar integrals have been classified and computed by 't Hooft and Veltman [55].

- **One-point Function**

  The relation

  $$A_0(m^2) = m^2[1 + B_0(0, m^2, m^2)] \tag{B.6}$$

  allows us to avoid using A_0 functions in our results. Therefore our decomposition includes two-,three- and four-point functions only.

- **Two-point Function**

  The two-point function B_0 is solved introducing a single Feynman parameter, resulting in a single squared polynomial in the loop momentum. Thus, the integration over the latter becomes straightforward as a logarithm and the integration of the Feynman parameter is carried out in terms of the roots of the logarithm polynomial argument. In particular, the two-point functions are UV divergent and, where the internal lines are fermionic, IR finite.

  For example,

  $$B_0(q^2, m^2, m^2) = \Delta_\epsilon - \log\left(\frac{m^2}{\mu^2}\right) + 2 - \sqrt{1 - \frac{4m^2}{q^2}} \log\left(\frac{\sqrt{1 - \frac{4m^2}{q^2}} + 1}{\sqrt{1 - \frac{4m^2}{q^2}} - 1}\right) \tag{B.7}$$

  where $\Delta_\epsilon = 2/\epsilon - \gamma + \log(4\pi)$. And we use the relation

  $$B_0(m^2, 0, m^2) = B_0(0, m^2, m^2) + 2. \tag{B.8}$$

- **Three-point Function**

  The three-point function is solved introducing two Feynman parameters, x and y, so the integral become

  $$C = i\pi^2 \int_0^1 dx \int_0^x dy [ax^2 + by^2 + cxy + dx + ey + f]^{-1}, \tag{B.9}$$

where the coefficients a, b, c, d, e and f depend on the arguments of C_0. At this stage we can perform a shift, that allow us to get rid of x via a straightforward integration and to write C_0 in terms of dilogarithms[2]:

$$Li_2(z) = -\int_0^z dt \frac{\log(1-t)}{t}. \tag{B.10}$$

Standard results in a cut-off regularization framework, compatible with our conventions, may be found in [72], appendix C. Here we only recall that the three-point functions are UV finite and, in our case, where at least one internal line is a photon propagator, IR divergent. The cases of our interest in which they are not IR divergent are highlighted in [56].

- **Four-point Function**

  The four-point function is solved introducing three Feynman parameters, but the computation is much more complicated than in the C_0 case. Moreover, there seems to be no simple formula covering the whole domain[3], including complex masses.

  If the masses are real, one can in most cases construct equations giving the four-point function in terms of 24 dilogarithms. Our four-point function are solved using the results of [72]. Other standard results for the four-point functions may be found in [56].

B.2   Bremsstrahlung

In computing soft bremsstrahlung one encounters an integral that is essentially a phase-space integral for photons with an energy less than some specified value. The basic integral is:

$$\mathcal{I}(p_i, p_j) = \int^{k^0 < \omega} \frac{d^3 k}{k^0} \frac{1}{(p_i \cdot k)(p_j \cdot k)} \qquad k^0 = \sqrt{\vec{k}^2 + \lambda^2}, \ \ |\vec{k}| < \omega. \tag{B.11}$$

Here λ is the photon mass, and p_i and p_j refer to four-momenta of the particles that emit the photon.

The integral with $p_i = p_j = p$ yields a direct calculation

$$
\begin{aligned}
\mathcal{I}(p, p) &= \int^{k^0 < \omega} \frac{d^3 k}{k^0} \frac{1}{(p \cdot k)^2} \\
&= 2\pi \int_0^\omega dk \frac{k^2}{\sqrt{\vec{k}^2 + \lambda^2}} \int_{-1}^1 d\cos\theta \frac{1}{m^2 \gamma^2 (\sqrt{\vec{k}^2 + \lambda^2} - \beta k \cos\theta)^2} \\
&\frac{4\pi}{m^2 \gamma^2} \int_0^\omega dk \frac{k^2}{\sqrt{\vec{k}^2 + \lambda^2}[(1 - \beta^2)k^2 + \lambda^2]} \\
&\simeq \frac{2\pi}{m^2} \left[2\log\frac{2\omega}{\lambda} - \frac{1}{\beta}\log\frac{1+\beta}{1-\beta} \right],
\end{aligned}
\tag{B.12}
$$

---

[2]Details of this computation are reported in section 5 of [55]

[3]Space-like, light-like and time-like external masses, and also if the internal masses have a constant imaginary part of a certain sign.

where m is the mass of the fermion, $\beta = |\vec{p}|/p^0$, $\gamma = 1/\sqrt{1-\beta^2}$ and $k \equiv |\vec{k}|$. The last equality holds in the limit $\lambda \to 0$, where $O(\alpha^2)$ terms may be neglected.

For the other cases, when p_i is not a multiple of p_j, the external momenta can be redefined as

$$p = \rho p_i \qquad q = p_j, \tag{B.13}$$

where ρ is chosen to satisfy $(p-q)^2 = 0$ and such that $p_0 - q_0$ has the same sign of q_0. Thus, one introduce a Feynman parameter x, thanks to this redefinition the calculation is simplified, but is still rather lengthy, therefore we only quote the result

$$\mathcal{I}\left(p_i, p_j\right) = -\frac{2\pi\rho}{vl} \left[\frac{1}{2} \log\left(\frac{p^2}{q^2}\right) \log\left(\frac{4\omega^2}{\lambda^2}\right) \right.$$
$$\left. + \left\{ \frac{1}{4} \log^2\left(\frac{u_0 - |\mathbf{u}|}{u_0 + |\mathbf{u}|}\right) + Li_2\left(\frac{v + u_0 + |\mathbf{u}|}{v}\right) + Li_2\left(\frac{v + u_0 - |\mathbf{u}|}{v}\right) \right\}_{u=q}^{u=p} \right] \tag{B.14}$$

with

$$l = p_0 - q_0, \qquad v = (p^2 - q^2)/2l, \qquad \lambda \to 0. \tag{B.15}$$

In particular, in the LAB frame, we have

$$p_1^0 = -\frac{m^2 + M^2 - s}{2s}, \qquad |\vec{p_1}| = \frac{\sqrt{m^4 - 2m^2(M^2 + s) + (M^2 - s)^2}}{2m}$$
$$p_2^0 = m,$$
$$p_3^0 = \frac{-m^2 - M^2 + s + t}{2m}, \qquad |\vec{p_3}| = \frac{\sqrt{m^4 - 2m^2(M^2 + s + t) + (-M^2 + s + t)^2}}{2m} \tag{B.16}$$
$$p_4^0 = m - \frac{t}{2m}, \qquad |\vec{p_4}| = \frac{\sqrt{t(t - 4m^2)}}{2m}.$$

Bibliography

[1] S. A. Goudschmidt and G. H. Uhlenbeck, Nature **117** (1926), 264-265.

[2] E. Back and A. Landé, "Zeemaneffekt und Multiplettstruktur der Spektrallinien", (J. Springer, Berlin, 1925), pp 213.

[3] P. A. M. Dirac, Proc. Roy. Soc. Lond. A **A117** (1928), 610-624.

[4] L. E. Kinsler and W. V. Houston, Phys. Rev. **45**, 104 (1934).

[5] J. S. Schwinger, Phys. Rev. **73** (1948), 416-417.

[6] C. M. Sommerfield, Phys. Rev. **107** (1957), 328-329.

[7] A. Petermann, Helv. Phys. Acta **30** (1957), 407-408.

[8] M. Passera, J. Phys. G **31** (2005), R75-R94.

[9] T. Aoyama *et al.* [arXiv:2006.04822 [hep-ph]].

[10] J. A. Mignaco and E. Remiddi Nuovo Cimento A **60** 519 (1969).
R. Barbieri and E. Remiddi, Phys. Lett. B **49** (1974), 468-470.
R. Barbieri and E. Remiddi, Nucl. Phys. B **90** (1975), 233-266.
R. Barbieri, M. Caffo and E. Remiddi, Phys. Lett. B **57** (1975), 460-462.
M. J. Levine, E. Remiddi and R. Roskies, Phys. Rev. D **20** (1979), 2068-2076.
S. Laporta and E. Remiddi, Phys. Lett. B **265** (1991), 182-184.
S. Laporta, Phys. Rev. D **47** (1993), 4793-4795.
S. Laporta, Phys. Lett. B **343** (1995), 421-426.
S. Laporta and E. Remiddi, Phys. Lett. B **356** (1995), 390-397.

[11] S. Laporta and E. Remiddi, Phys. Lett. B **379** (1996), 283-291.

[12] S. Laporta, Nuovo Cim. A **106** (1993), 675-683.

[13] S. Laporta and E. Remiddi, Phys. Lett. B **301** (1993), 440-446.

[14] M. Caffo, S. Turrini and E. Remiddi, Phys. Rev. D **30** (1984), 483.
E. Remiddi and S. P. Sorella, Lett. Nuovo Cim. **44** (1985), 231.
D. J. Broadhurst, A. L. Kataev and O. V. Tarasov, Phys. Lett. B **298** (1993), 445-452.

S. Laporta, Phys. Lett. B **312** (1993), 495-500.
P. A. Baikov and D. J. Broadhurst, [arXiv:hep-ph/9504398 [hep-ph]].

[15] T. Kinoshita and W. B. Lindquist, Phys. Rev. D **42** (1990), 636-655.

[16] T. Kinoshita, B. Nizic and Y. Okamoto, Phys. Rev. Lett. **52** (1984), 717.

[17] S. Laporta, Phys. Lett. B **772** (2017), 232-238.

[18] B. E. Lautrup, Phys. Lett. B **38** (1972), 408-410.

[19] T. Aoyama, M. Hayakawa, T. Kinoshita and M. Nio, Phys. Rev. Lett. **109** (2012), 111808.

[20] A. Kurz, T. Liu, P. Marquard and M. Steinhauser, Nucl. Phys. B **879** (2014), 1-18 [arXiv:1311.2471 [hep-ph]].

[21] R. H. Parker, C. Yu, W. Zhong, B. Estey and H. Müller, Science **360** (2018), 191.

[22] R. Jackiw and S. Weinberg, Phys. Rev. D **5** (1972), 2396-2398.
I. Bars and M. Yoshimura, Phys. Rev. D **6** (1972), 374-376.
G. Altarelli, N. Cabibbo and L. Maiani, Phys. Lett. B **40** (1972), 415-419.
W. A. Bardeen, R. Gastmans and B. E. Lautrup, Nucl. Phys. B **46** (1972), 319-331.
K. Fujikawa, B. W. Lee and A. I. Sanda, Phys. Rev. D **6** (1972), 2923-2943.

[23] A. Czarnecki, B. Krause and W. J. Marciano, Phys. Rev. D **52** (1995), 2619-2623.

[24] A. Czarnecki, B. Krause and W. J. Marciano, Phys. Rev. Lett. **76** (1996), 3267-3270.

[25] T. Kaneko and N. Nakazawa, [arXiv:hep-ph/9505278 [hep-ph]].

[26] A. Czarnecki, W. J. Marciano and A. Vainshtein, Phys. Rev. D **67** (2003), 073006.

[27] C. Gnendiger, D. Stöckinger and H. Stöckinger-Kim, Phys. Rev. D **88** (2013), 053005.

[28] T. Ishikawa, N. Nakazawa and Y. Yasui, Phys. Rev. D **99** (2019) no.7, 073004.

[29] M. Tanabashi *et al.* [Particle Data Group], Phys. Rev. D **98** (2018) no.3, 030001.

[30] C. Bouchiat and L. Michel, J. Phys. Radium **22** (1961) no.2, 121-121.

[31] M. Davier, A. Hoecker, B. Malaescu and Z. Zhang, Eur. Phys. J. C **77** (2017) no.12, 827.
A. Keshavarzi, D. Nomura and T. Teubner, Phys. Rev. D **97** (2018) no.11, 114025.
G. Colangelo, M. Hoferichter and P. Stoffer, JHEP **02** (2019), 006.
M. Hoferichter, B. L. Hoid and B. Kubis, JHEP **08** (2019), 137.
M. Davier, A. Hoecker, B. Malaescu and Z. Zhang, Eur. Phys. J. C **80** (2020) no.3, 241.

[32] A. Keshavarzi, D. Nomura and T. Teubner, Phys. Rev. D **101** (2020) no.1, 014029 doi:10.1103/PhysRevD.101.014029 [arXiv:1911.00367 [hep-ph]].

[33] G. W. Bennett *et al.* [Muon g-2], Phys. Rev. Lett. **92** (2004), 161802.

[34] J. Grange *et al.* [Muon g-2], [arXiv:1501.06858 [physics.ins-det]].
G. Venanzoni [Fermilab E989], Nucl. Part. Phys. Proc. **273-275** (2016), 584-588 [arXiv:1411.2555 [physics.ins-det]].

[35] N. Saito [J-PARC g-'2/EDM], AIP Conf. Proc. **1467** (2012), 45-56.
T. Mibe [J-PARC g-2], Nucl. Phys. B Proc. Suppl. **218** (2011), 242-246.
M. Abe *et al.* PTEP **2019** (2019) no.5, 053C02 [arXiv:1901.03047 [physics.ins-det]].

[36] C. Aubin and T. Blum, Phys. Rev. D **75** (2007), 114502.
P. Boyle, L. Del Debbio, E. Kerrane and J. Zanotti, Phys. Rev. D **85** (2012), 074504.
X. Feng, K. Jansen, M. Petschlies and D. B. Renner, Phys. Rev. Lett. **107** (2011), 081802.
M. Della Morte, B. Jager, A. Juttner and H. Wittig, JHEP **03** (2012), 055.
T. Blum *et al.* Phys. Rev. Lett. **116** (2016) no.23, 232002.
B. Chakraborty, C. T. H. Davies, P. G. de Oliviera, J. Koponen, G. P. Lepage and R. S. Van de Water, Phys. Rev. D **96** (2017) no.3, 034516.

[37] C. M. Carloni Calame, M. Passera, L. Trentadue and G. Venanzoni, Phys. Lett. B **746** (2015), 325-329.

[38] G. Abbiendi, C. M. Carloni Calame, U. Marconi, C. Matteuzzi, G. Montagna, O. Nicrosini, M. Passera, F. Piccinini, R. Tenchini, L. Trentadue and G. Venanzoni, Eur. Phys. J. C **77** (2017) no.3, 139.

[39] The MUonE Collaboration, *Letter of Intent: The MUonE Project*, CERN SPSC-2019-026/SPSC-I-252. https://cds.cern.ch/record/2677471/files/SPSC-I-252.pdf

[40] A. Masiero, P. Paradisi and M. Passera, [arXiv:2002.05418 [hep-ph]].

[41] P. S. B. Dev, W. Rodejohann, X. J. Xu and Y. Zhang, JHEP **05** (2020), 053 [arXiv:2002.04822 [hep-ph]].

[42] R. V. Harlander and M. Steinhauser, Comput. Phys. Commun. **153** (2003), 244-274.

[43] G. Abbiendi *et al.*, JINST **15** (2020) no.01, 01.

[44] P. Banerjee *et al.* Eur. Phys. J. C **80** (2020) no.6, 591.

[45] A. I. Nikishov Sov. Phys. JETP **12** (1961), 529.

[46] K. E. Eriksson, Nuovo Cim. **19** (1961) 1029.

[47] K. E. Eriksson, B. Larsson and G. A. Rinander, Nuovo Cim. **30** (1963) 1434.

[48] P. Van Nieuwenhuizen, Nucl. Phys. B **28** (1971), 429-454.

[49] G. D'Ambrosio, Lett. Nuovo Cim. **38** (1983), 593-598.

[50] D. Y. Bardin and L. Kalinovskaya, [arXiv:hep-ph/9712310 [hep-ph]].

[51] T. V. Kukhto, N. M. Shumeiko and S. I. Timoshin, J. Phys. G **13** (1987) 725.

[52] N. Kaiser, J. Phys. G **37** (2010), 115005.

[53] M. Alacevich, C. M. Carloni Calame, M. Chiesa, G. Montagna, O. Nicrosini and F. Piccinini, JHEP **02** (2019), 155.

[54] R. Mertig, M. Bohm and A. Denner, Comput. Phys. Commun. **64** (1991), 345-359; V. Shtabovenko, R. Mertig and F. Orellana, Comput. Phys. Commun. **207** (2016), 432-444 [arXiv:1601.01167 [hep-ph]].

[55] G. 't Hooft and M. J. G. Veltman, Nucl. Phys. B **153** (1979), 365-401.

[56] R. K. Ellis and G. Zanderighi, JHEP **02** (2008), 002.

[57] Z. Bern, L. J. Dixon and A. Ghinculov, Phys. Rev. D **63** (2001), 053007.

[58] R. Bonciani, P. Mastrolia and E. Remiddi, Nucl. Phys. B **661** (2003), 289-343.

[59] R. Bonciani, A. Ferroglia, P. Mastrolia, E. Remiddi and J. J. van der Bij, Nucl. Phys. B **681** (2004), 261-291.

[60] R. Bonciani, A. Ferroglia, T. Gehrmann, D. Maitre and C. Studerus, JHEP **07** (2008), 129.

[61] R. Bonciani, A. Ferroglia, T. Gehrmann, A. von Manteuffel and C. Studerus, JHEP **12** (2013), 038.

[62] P. Mastrolia, M. Passera, A. Primo and U. Schubert, JHEP **11** (2017), 198.

[63] S. Di Vita, S. Laporta, P. Mastrolia, A. Primo and U. Schubert, JHEP **09** (2018), 016.

[64] S. Di Vita, T. Gehrmann, S. Laporta, P. Mastrolia, A. Primo and U. Schubert, JHEP **06** (2019), 117.

[65] T. Engel, C. Gnendiger, A. Signer and Y. Ulrich, JHEP **02** (2019), 118.

[66] P. Banerjee, T. Engel, A. Signer and Y. Ulrich, SciPost Phys. **9** (2020), 027.

[67] C. M. Carloni Calame, M. Chiesa, S. M. Hasan, G. Montagna, O. Nicrosini and F. Piccinini, [arXiv:2007.01586 [hep-ph]].

[68] M. Fael and M. Passera, Phys. Rev. Lett. **122** (2019) no.19, 192001.

[69] M. Fael, JHEP **02** (2019), 027.

[70] H. H. Patel, Comput. Phys. Commun. **218** (2017), 66-70 [arXiv:1612.00009 [hep-ph]].

[71] G. Passarino and M. J. G. Veltman, Nucl. Phys. B **160** (1979), 151-207.

[72] W. Beenakker and A. Denner, Nucl. Phys. B **338** (1990), 349-370.

Acknowledgements

This thesis represents the final aim of these years of study in Padova. It's been a long journey, but, finally, I am standing on the goal line. Before taking the last step and begin a new adventure, I want to thank all people that have shared the way with me.

Firstly my family: my father Dino, my mother Agnese and my sister Silvia, that have always sustained me in all the aspects of my life and have known how to give fundamental pieces of advise at the right moment to lead me on the right path.

Secondly, I want to thank all my friends: Federica, Jessica, Linda, Martina, Gloria and Elisa. I mean, I known you all my life and you have always supported your crazy physicist friend. And I know that I can always count on you.

A special mention goes to my thesis advisor Prof. Massimo Passera, that, despite the distance, has always been the right person to ask how to solve any kind of problem that arose during the development and writing of this work, helping me when I needed. Thanks also for assist me in PhD applications, I very appreciated that.

I want also to thank my "University friends", who accompanied me in this journey, from the beginning in Parma to the end in Padova. In particular I want to thank my "physicist sister" Carlotta, it seems like only yesterday that we were studying together Geometry 1, from that moment you have always been by my side. I couldn't do it without your support.

Last but not least, I want to thank my other half Manuel, with whom I have passed the most beautiful eight years of my life. You have always known how to cheer me up in bad moments and how to make good ones even better. You have never doubted of my ability, encouraging me to always give the best.